

Aspects of Machian Gravity (III): Testing Theory against Galaxy Cluster mass

Santanu Das

Theoretical Physics Group, Blackett Laboratory,
Imperial College London, SW7 2AZ, UK

E-mail: santanu.das@imperial.ac.uk

Abstract. The general theory of relativity (GR) has excelled in explaining gravitational phenomena at the scale of the solar system with remarkable precision. However, when extended to the galactic or cosmological scale, it requires dark matter and dark energy to explain observations. In our previous article ([arXiv:2308.04503](https://arxiv.org/abs/2308.04503)), we've formulated a gravity theory based in Mach's principle, known as Machian gravity. We demonstrated that the theory successfully explains galactic velocity profiles without requiring additional dark matter components. In previous studies, for a selected set of galaxy clusters, we also showed its ability to explain the velocity dispersion in the clusters without extra unseen matter components. This paper primarily explores the mass profiles of galaxy clusters. We test the Machian Gravity acceleration law on two distinct sets comprising approximately 150 galaxy clusters sourced from various studies. We fitted the dynamic mass profiles using the Machian gravity model. The outcomes of our study show exceptional agreement between the theory and observational results.

Contents

1	Introduction	1
2	Machian gravity an overview	2
3	A theoretical background of galaxy clusters	3
3.1	Galactic cluster mass	4
3.2	Calculating β , r_c and ρ_0	4
4	Analysis and Results	6
4.1	Fitting with three parameters	8
5	Discussion and Conclusion	10

1 Introduction

The mystery of galaxy rotation curves and galaxy cluster masses has long perplexed physicists, as it requires some form of additional matter that makes its presence filled by gravitational effects. The most intuitive solution to this is adding additional invisible matter, otherwise known as dark matter. However, dark matter does not solve all the issues. For instance, it has been seen that for every feature in the rotation curve of a galaxy, there is a consecutive feature in the light curve [1]. Provided there is an independent dark matter that is not coupled with the baryon, it's impossible to explain these observations.

Several modified gravity theories have emerged over years. Milgrom proposed MOND, altering Newtonian dynamics to explain galactic velocity profiles [2–5]. Bekenstein introduced AQUAL, providing a mathematical foundation for MOND [6–8]. However, MOND falls to explain galaxy cluster mass profiles, necessitating additional dark matter components. Moffat proposed MoG, bridging this gap without invoking dark matter [9–12]. Other theories, including TeVeS [13], Massive Gravity [14–17], and higher-dimensional theories such as Induced Matter Theory [18–22], have also been proposed.

While some existing theories can account for the missing masses without invoking additional dark matter components, these solutions primarily stem from attempts to explain observed phenomena rather than originating from fundamental frameworks like general relativity. In our prior research, we proposed a gravitational theory based on Mach's principle. This is a metric theory based on a 5-dimensional spacetime [23]. The theory demonstrates remarkable explanatory power in explaining various phenomena, such as spiral galactic velocity profiles, velocity dispersion in galaxy clusters, and cosmological expansion history, etc. [23, 24]. This paper demonstrates the explanatory power of the theory on a larger sample of galaxy cluster.

Galaxy clusters are objects that form in locations corresponding to peaks in the initial mass distribution. They are the largest bound masses, which account for a larger fraction of mass content in the Universe. It is believed that 80-90% of the matter content in these clusters is in the form of dark matter interacting only through gravity. Galaxies that we observe in the electromagnetic spectrum, including their stellar components and the intergalactic gas (shining in X-rays), account for the remaining 10-20% of matter present. In this paper, we investigate how Machian Gravity can address the missing mass corresponding to galaxy clusters.

The article has been organized as follows. In the second section, we have briefly described the Machian gravity theory in the limits of the galactic clusters. The third section discusses the details of the measurements involved in the galactic clusters. In the next section, we discuss various analyses and results. We fit the Machian Gravity formula on two data sets. The first data set consists of 106 X-ray clusters compiled from XMM-Newton data [25]. We have shown a parametric fit to the data using the

same acceleration law, which was earlier used to explain the galactic velocity profile, can explain the velocity dispersion in the clusters. Here, we like to mention that the MOND-like acceleration law fails to explain the cluster mass and requires additional dark matter components [26]. We then slightly modify the acceleration law based on the data from the first set and apply it to another set of data comprised of 44 clusters compiled from Chandra X-ray telescope data [32]. This modified acceleration law shows an excellent fit for the data. The final section provides a comprehensive discussion and conclusion, underscoring the significance of Machian gravity.

2 Machian gravity an overview

Machian gravity is fundamentally based on Mach's principle, a concept that challenges our understanding of inertia on a fundamental level. Despite being a cornerstone of physics, mass lacks a precise definition. It can be approached from two angles: inertial mass, which pertains to its resistance to acceleration, and gravitational mass, which concerns its gravitational interactions. A comprehensive overview of this can be found in [27].

To accurately determine the inertial mass of a particle, it is necessary to establish an inertial reference frame. However, it is difficult, or maybe impossible, to determine the inertial reference frame because there is no external reference frame based on which its acceleration can be measured. To overcome this, Ernest Mach proposed that the inertial reference frame can be determined based on the motions of distant objects in the universe. This implies that the distant objects in the universe actually determine the inertial properties of matter, which is the famous Mach's principle. Therefore, if two identical objects are placed at different locations in the universe, their inertial properties may differ depending on their backgrounds. Two identical particles may have different inertial masses or experience different forces due to their background.

A famous example of this is Newton's bucket experiment. Imagine a bucket filled with water that is rotating. Due to the centripetal force, the water's surface curves. However, if we define the coordinate system on the bucket, then the water is fixed on that coordinate system, which means there is no centripetal force acting on it. Therefore, the surface should be flat. However, that is not the case. The new reference frame is non-inertial, which means that we need to add some additional fictitious forces to balance the forces, in this case, the centrifugal force to be particular. However, we don't know the source of this force. According to Mach's principle, in this new reference frame, the rest of the universe (all stars, galaxies, etc.) is also rotating. Therefore, due to this rotation, the rest of the universe is somehow creating a force on the reference frame, which is responsible for the centrifugal force.

In our previous work, we have shown that in a 5-dimensional coordinate frame, we can recover all these inertial forces from the background [23]. In a vacuum, the field equation for the theory is given by $\tilde{G}_{AB} = 0$, where A, B varies from 0 to 4, and the tilde represents that the quantities are in 5 dimensional spacetime. This, after some rearrangements, can be written as $\tilde{R}_{AB} = 0$, where \tilde{R}_{AB} is the Ricci tensor. Let us assume that the perturbation in the metric due to the gravitational field is $\tilde{\gamma}_{AB}$. For this weak field limit, only $\tilde{R}_{00} = \tilde{R}_{0C0}^C$ is the important term, as all the other components are of the order of $O(1/c)$ or less, where the term on the right-hand side is the Riemann tensor.

$$\tilde{R}_{0A0}^B = \partial_A \tilde{\Gamma}_{00}^B - \partial_0 \tilde{\Gamma}_{A0}^B + \tilde{\Gamma}_{AC}^B \tilde{\Gamma}_{00}^C - \tilde{\Gamma}_{0C}^B \tilde{\Gamma}_{A0}^C \quad (2.1)$$

The second term here is a time derivative, which vanishes for static fields. The third and fourth terms are of the form $(\tilde{\Gamma})^2$, and since $\tilde{\Gamma}$ is first-order in the metric perturbation, these contribute only at second order and can be neglected, giving

$$\tilde{R}_{00} = \tilde{R}_{0A0}^A = \partial_A \left(\frac{1}{2} \tilde{g}^{AC} (\partial_0 \tilde{g}_{C0} + \partial_0 \tilde{g}_{0C} - \partial_C \tilde{g}_{00}) \right) = -\frac{1}{2} \tilde{g}^{AB} \partial_A \partial_B \tilde{\gamma}_{00} \quad (2.2)$$

For the static solution, the time derivative also vanishes, and the equation becomes

$$\partial_\zeta^2 \tilde{\gamma}_{00} + \partial_x^2 \tilde{\gamma}_{00} + \partial_y^2 \tilde{\gamma}_{00} + \partial_z^2 \tilde{\gamma}_{00} = 0. \quad (2.3)$$

Here ζ is the fifth coordinate. Under the assumption of spherical symmetry of the special part, it can be written as

$$\partial_\zeta^2(r\tilde{\gamma}_{00}) + \partial_r^2(r\tilde{\gamma}_{00}) = 0. \quad (2.4)$$

Using ‘separation of variables’ and considering $(r\tilde{\gamma}_{00}) = R(r)\chi(\zeta)$, we get

$$\frac{1}{R} \frac{\partial^2 R}{\partial r^2} = -\frac{1}{\chi} \frac{\partial^2 \chi}{\partial \zeta^2} = \lambda^2, \quad (2.5)$$

where, λ is a constant. To relate it with Newtonian gravity, we can put $\tilde{\gamma}_{00} = 2\Phi$, where Φ is the Newtonian potential of the gravitational field. Few straightforward manipulations lead us to

$$\Phi = \frac{GM}{r} [1 + K(1 - e^{-\lambda r})]. \quad (2.6)$$

Here, M is the enclosed mass within radius r . G is the Newton’s gravitational constant. λ and K are the quantities that depend on the background mass distribution. They may depend on mass M but are independent on r . Galactic velocity profiles show that λ is of the order of few kpc^{-1} . When r is small, $e^{-\lambda r} \sim 1$, Φ takes the form of Newtonian potential i.e. $\Phi = \frac{GM}{r}$. This gives the Newtonian gravitational equation at the solar system scale. In the asymptotic limit of $r \rightarrow \infty$, the exponential term goes to 0. Hence, for large values of r , it becomes $(1 + K)$ times that of Newtonian potential and can provide additional gravitational force in large gravitationally balanced systems, such as galaxies. In fact, a similar form of potential has previously been used by other groups to explain the galactic velocity profile [9–12, 28].

In our previous work cited as [23, 24], we demonstrated that when a particle orbits in a circular path in this potential, the velocity curve flattens out when $\lambda r \in (0.4, 2.5)$ and $K \in (11, 19)$. This flattened-out velocity profile can be used to explain the rotational velocity profile of the outer edge of a galaxy. We used the equation $K = \left(\frac{M_c}{M}\right)^\alpha - 1$ to recover the baryonic Tully-Fisher relation for spiral galaxies. In this equation, M_c represents a constant mass and α is some power law power. When we take $\alpha = \frac{1}{2}$, it gives the baryonic Tully-Fisher relation, given by $v^4 \propto M$. This gives us the velocity in a circular orbit as

$$v^2 = \frac{GM}{r} \left[1 + \left(\sqrt{\frac{M_c}{M}} - 1 \right) (1 - e^{-\lambda r} (1 + \lambda r)) \right]. \quad (2.7)$$

It’s important to note that the term enclosed within the bracket relies on the background mass distribution. Otherwise, it would violate the symmetry argument. For instance, in a scenario with only two particles, the gravitational attraction between them would obey Newtonian laws, i.e. the resulting force should be symmetric about both masses. In this case, the term enclosed within the bracket would be unity. However, in the presence of a mass distribution, such as in galaxies or galaxy clusters, the term within the bracket varies depending on the specific mass distribution. We don’t have an exact form of K from our equations. Hence, we resort to using a power law with a power $\alpha \approx 0.5$.

3 A theoretical background of galaxy clusters

Clusters of galaxies are believed to comprise three primary components. Galaxy clusters, as suggested by their name, have been identified as groupings of galaxies. Each cluster can contain roughly 100-1000 galaxies, constituting approximately 1% of its mass. The expanse between these galaxies is not devoid of matter; instead, it contains substantial amounts of intracluster gas (ICG), comprising about 9%. The predominant portion of the overall gravitational mass in clusters is believed to exist in the form of dark matter, accounting for the remaining 90% (based on calculations employing Newtonian Mechanics). Of course in modified gravity theories the dark matter components will not exist.

3.1 Galactic cluster mass

The density distribution of hot gas in a cluster has been well described by the King β -model [11, 29, 30].

$$\rho(r) = \rho_0 \left[1 + \left(\frac{r}{r_c} \right)^2 \right]^{-3\beta/2}, \quad (3.1)$$

where ρ_0 is the central density and r_c is a core radius. Here β is known as the shape parameter. By fitting this model to the mean radial profile of X-ray surface brightness in clusters, the quantity β can be found. While the assumptions of the β -model may not be completely accurate, the surface brightness profile derived from it represents the measured profile well within a wide range, which makes this model widely accepted.

The mass profile of the cluster can be calculated by integrating the density profile, i.e.

$$M_b(r) = 4\pi \int_0^r \rho(r') r'^2 dr'. \quad (3.2)$$

We can integrate it numerically to get the gas mass of the galaxy cluster. For large radii and small β values we can an approximate analytical formula for the gas mass as

$$M_b(r) \approx \frac{4\pi\rho_0 r_c^3}{-3\beta + 3} \left(\frac{r}{r_c} \right)^{-3\beta+3} \quad \frac{r}{r_c} \gg 1, \beta < 1. \quad (3.3)$$

Here we should note that the above function is a divergent function for $\beta > 1$. Therefore, we must have $\beta < 1$.

3.2 Calculating β , r_c and ρ_0

Intracluster gas (ICG) is trapped and heated to $10^7 - 10^8$ K in the cluster gravitational potential. Thermal bremsstrahlung emission from this ICG makes clusters luminous X-ray sources. The main constituents of the ICG are the Hydrogen and Helium, where a good approximation of the number densities is $n_{He} = n_H/10$. Due to the high temperature the gas can be considered completely ionized and mean molecular weight including the electrons

$$\mu \approx \frac{1 + 2 \sum_{Z>1} w_Z Z}{2 + \sum_{Z>1} w_Z (Z + 1)}, \quad (3.4)$$

where Z is the atomic number and w_Z the the relative weight e.g., $w_2 = 0.1$ and $w_Z = 0$ for $Z > 2$. This gives $\mu \approx 0.61$ and $\rho(r) \approx 1.17n_e m_p$. Therefore, the electron number density should also follow the relation

$$n_e(r) = n_{e0} \left[1 + \left(\frac{r}{r_c} \right)^2 \right]^{-3\beta/2}. \quad (3.5)$$

For the X-ray surface brightness, i.e. the number of photons detected in a defined energy range per unit time and per unit solid angle, one has

$$S \propto \int_{-\infty}^{\infty} n_e^2 dl \quad \implies \quad S \propto \int_{-\infty}^{\infty} \left[1 + \left(\frac{r}{r_c} \right)^2 \right]^{-3\beta} dl, \quad (3.6)$$

where the integration in along the light of sight. This integral can be reduced to a form

$$S(R) = S_0 \left[1 + \left(\frac{R}{r_c} \right)^2 \right]^{-3\beta + \frac{1}{2}}, \quad (3.7)$$

Here R denotes as the projected distance from the center of the cluster. This can be fitted with the observed surface brightness profile and measure the values for S_0 , r_c and β . Thereby ρ_o can be calculated. The measured values of these for different clusters are taken from [25].

For calculating the total gas mass of a cluster, we also need the outer radius of the cluster. The above equation holds to a point where the cluster X-ray emission is lost in the background [31]. For parametric analysis, define the outer radius of the cluster as the radius where the density of the cluster is about 250 times the cosmological baryon density, and this radius is taken as r_{250} . So, from Eq. 3.2, we can get the total baryonic gas mass of the galaxy cluster.

Dynamic mass of a galaxy The basic assumption that is taken for calculating the dynamic mass of a cluster is that the gas inside the cluster is in hydrostatic equilibrium, which gives

$$\frac{dP(r)}{dr} = -\frac{\rho(r)GM_d(r)}{r^2} \quad (3.8)$$

where $P(r)$ represents the gas pressure, G is the gravitational constant. $M_d(r)$ is the gravitating mass of the cluster inside a radius r . With the ideal gas equation,

$$P = \frac{k_B}{\mu m_p} \rho T, \quad (3.9)$$

this leads to

$$M_d(r) = \frac{k_B T r^2}{\mu m_p G} \left(\frac{1}{\rho(r)} \frac{d\rho(r)}{dr} + \frac{1}{T(r)} \frac{dT(r)}{dr} \right). \quad (3.10)$$

where T is the temperature of the cluster, m_p is the mass of proton, $\mu = 0.609$ is mean atomic weight and k is the Boltzmann constant. From XMM-Newton it is also seen that the clusters are isothermal at least up to half of the virial radius. In this analysis we consider the clusters to be completely isothermal. For isothermal clusters, we can take the temperature derivative to be 0. Putting the value of $\rho(r)$ we get the dynamical mass of the cluster as

$$M_d(r) = \frac{3\beta k T}{\mu m_p G} \left(\frac{r^3}{r^2 + r_c^2} \right). \quad (3.11)$$

Machian Gravity Formulation Under Machian gravity, the gravitational equation will change. As we have not considered any dark matter, the matter component will be given by the baryonic component only. Therefore, by putting the gravitational equation in the hydrostatic equilibrium equation and doing similar analysis, we get

$$M_b(r) \{1 + K [1 - \exp(-\lambda r) (1 + \lambda r)]\} = \frac{3\beta k T}{\mu m_p G} \left(\frac{r^3}{r^2 + r_c^2} \right), \quad (3.12)$$

K and λ are the background dependent quantities. Earlier, for explaining the spiral galactic Tully-Fisher relation, we used $K = \left(\sqrt{\frac{M_c}{M_b(r)}} - 1 \right)$. However, it does not imply that galaxy clusters should also follow a similar relation because the mass distribution is different than spiral galaxies. Secondly, they are gravitationally bound systems, while galaxy clusters are supported by hydrostatic equilibrium.

As λ^{-1} is of the order of 10s to 100s of kpc, as can be seen for galaxy velocity profile study [24], at the edge of the clusters, we can expect $\exp(-\lambda r) \rightarrow 0$. There the equation will take the form

$$M_b(r_{out})(1 + K) = \frac{3\beta k T}{\mu m_p G} \left(\frac{r_{out}^3}{r_{out}^2 + r_c^2} \right), \quad (3.13)$$

where r_{out} is the outer radius of the cluster.

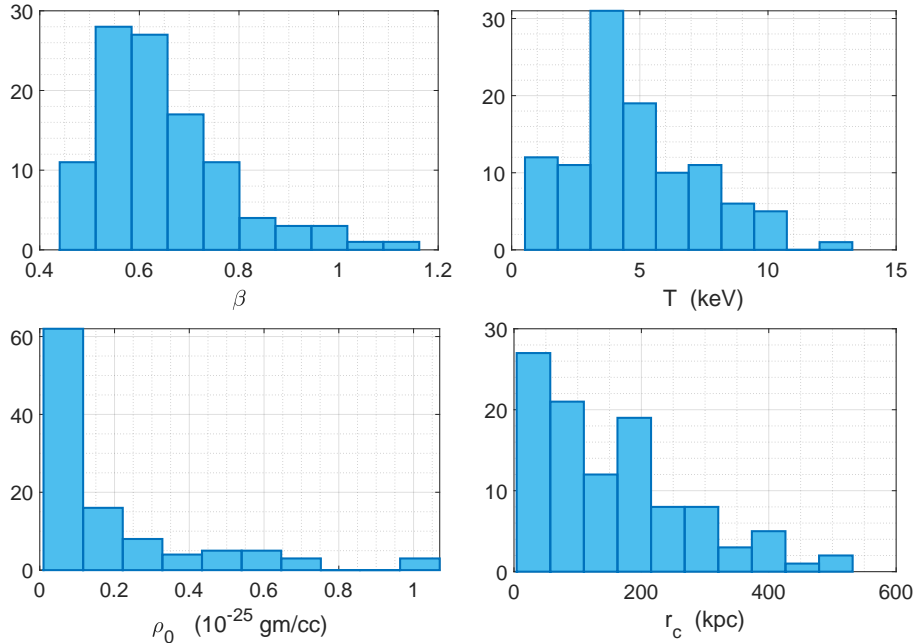


Figure 1. We can observe the distribution of various properties of 106 galaxy clusters in the plot. The distribution of β appears smoother, with a peak at approximately $\beta = 0.56$. In the top right plot, the isothermal temperature of the cluster has a slightly flatter distribution, with a maximum value at around 4 keV. Although the density at the core of the clusters can vary significantly, it is less than 0.1×10^{-25} gm/cc for over 60% of the clusters. Finally, the core radius r_c also varies significantly between different clusters.

4 Analysis and Results

We have analyzed our results with two sets of samples. The first set consists a total of 106 galaxy clusters taken from [25]. The properties of the sample with their error bars are shown in the table 1. For understanding the sample, in Fig. 1 we have plotted the distribution of β , T , ρ_0 , r_c for all the clusters. We can see that the β is roughly centered around 0.6483 ± 0.1349 . The temperature distribution of the clusters is roughly flat between (0, 10)keV with a peak at about 4 – 5keV. For most of the clusters, ρ_0 is less than 0.2 gm/cc and r_c , i.e. the core radius of the cluster is mostly within 500kpc. The outer radius of the cluster, r_{out} , is taken as the radius where the density of the cluster is about 250 times the cosmological baryon density. We use Eq. 3.2 to calculate the baryon mass in the galaxy cluster. As β centered around 0.65, at $\frac{r}{r_c} \gg 1$, the baryonic mass go as $M_b(r) \sim r^{1.05}$ for most of the clusters according to the Eq. 3.3. The dynamic mass (calculated from Newtonian mechanics) is given by Eq. 3.10, and for $r \gg r_c$, the dynamic mass $M_d(r) \sim r$ as given by Eq. 3.11. Therefore, roughly, we can see that for $r \gg r_c$, the ratio of the dynamic mass and the baryonic mass becomes almost independent of r for the mean radius. However, for different galaxy clusters, the ratio may depend on different powers of r .

The total baryon mass and dynamic mass of the galaxy cluster upto radius r_{250} is taken as M_{b250} and M_{d250} . In Fig. 2, we have plotted the temperature of the 106 clusters as a function of M_{b250} . The best-fit regression lines give

$$\log(T) = 0.43 \log(M_{b250}) + 0.82, \quad (4.1)$$

i.e. roughly $M_{b250} \sim T^2$ which is in agreement with previous analysis [31]. The ratio of the Newtonian dynamic mass, M_{d250} , and M_{b250} is roughly constant, which is about 10. However, there is a slight

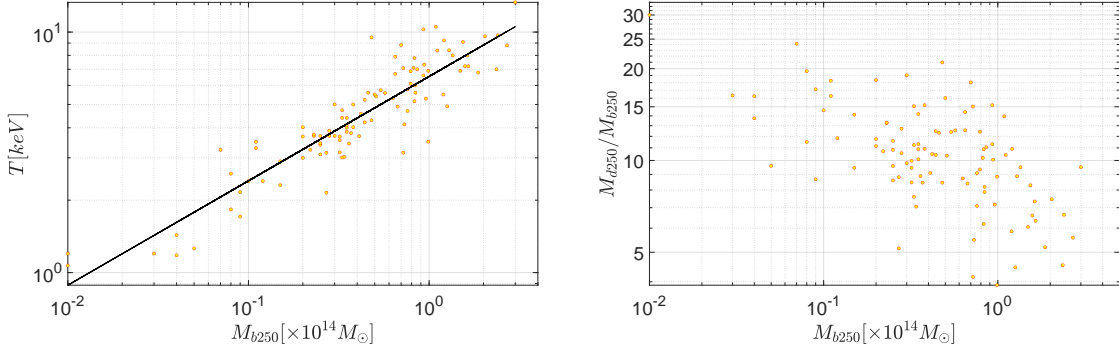


Figure 2. The plot illustrates various characteristics of the clusters. On the left, the graph depicts the relationship between T and M_{b250} . The black curve represents the best-fit regression line derived from the data points, indicating an approximately quadratic dependence, with $M_{b250} \propto T^2$. On the right, the plot demonstrates M_{d250}/M_{b250} as a function of M_{b250} . It is exhibiting a slight negative correlation, the ratio remains relatively constant (about 10) across the range of M_{b250} values.

negative correlation between the ratio and the $\log(M_{b250})$. A regression fit to the total dynamic mass and the baryonic mass is given by

$$\log(M_{d250}) = 0.7 \log(M_{b250}) + 3.87. \quad (4.2)$$

From Eq. 3.11, Eq. 3.13 we can get that at the outer edge of a galaxy cluster $M_d \propto M_b(1 + K)$. Therefore, the above relation shows that for clusters $K = \left(\frac{M_c}{M_b}\right)^{0.3} - 1$ may provide a better fit than the square root relation, assuming M_c is constant. However, the mass distribution of each galaxy cluster can be different. Therefore, there is no reason that M_c can be constant. Therefore, we fit this first set of data with the same square root relation as used for explaining the galaxy velocity profiles. Our analysis shows that the relation fits the galaxy cluster mass profiles well.

We fit the left-hand side of Eq. 3.12 against the Newtonian dynamic mass of the cluster given by Eq. 3.11 and optimize M_c and λ^{-1} by minimizing the χ^2 given by

$$\chi^2 = \sum_i \left[M_d(r_i) - M_b(r_i) \left[1 + \left(\sqrt{\frac{M_c}{M_b(r_i)}} - 1 \right) (1 - e^{-\lambda r_i} (1 + \lambda r_i)) \right] \right]^2 / \Delta M_d(r_i)^2. \quad (4.3)$$

We divided the entire radius into 100 logarithmic spacing points. In each point, we calculate the dynamic and the baryonic mass. The upper and lower error bars of M_d are calculated from the error bars of β and T . We use the root mean square of these two error bars in the χ^2 formula. Fig. 3 shows how the value of best fit M_c and λ^{-1} varies as a function of M_{b250} and r_c . We can see a very strong correlation between M_c and M_{b250} . As M_c depends on the mass distribution, intuitively, we may expect a correlation between M_c and M_{b250} . The relation is given by

$$\log(M_c) = 0.4776 \log(M_{b250}) + 0.4649. \quad (4.4)$$

However, without a proper theory of gravity and without knowing how the background affects gravity, it's impossible to know the exact relation. This result also aligned with the previous result in Eq. 4.2, where we had seen that a better fit will be $K+1 \propto M_{b250}^{-0.3}$, while Eq. 4.4, we get $K+1 \propto M_{b250}^{(0.48-1)/2} = M_{b250}^{-0.26}$. Our results show that λ^{-1} is almost independent on M_b . We have also plotted M_c and λ^{-1} against the core radius of the clusters, r_c . Both of them show a positive correlation. The best-fit regression lines give

$$\log(M_c) = 0.6988 \log(r_c) - 1.1643, \quad \log(\lambda^{-1}) = 0.8652 \log(r_c) - 0.0019. \quad (4.5)$$

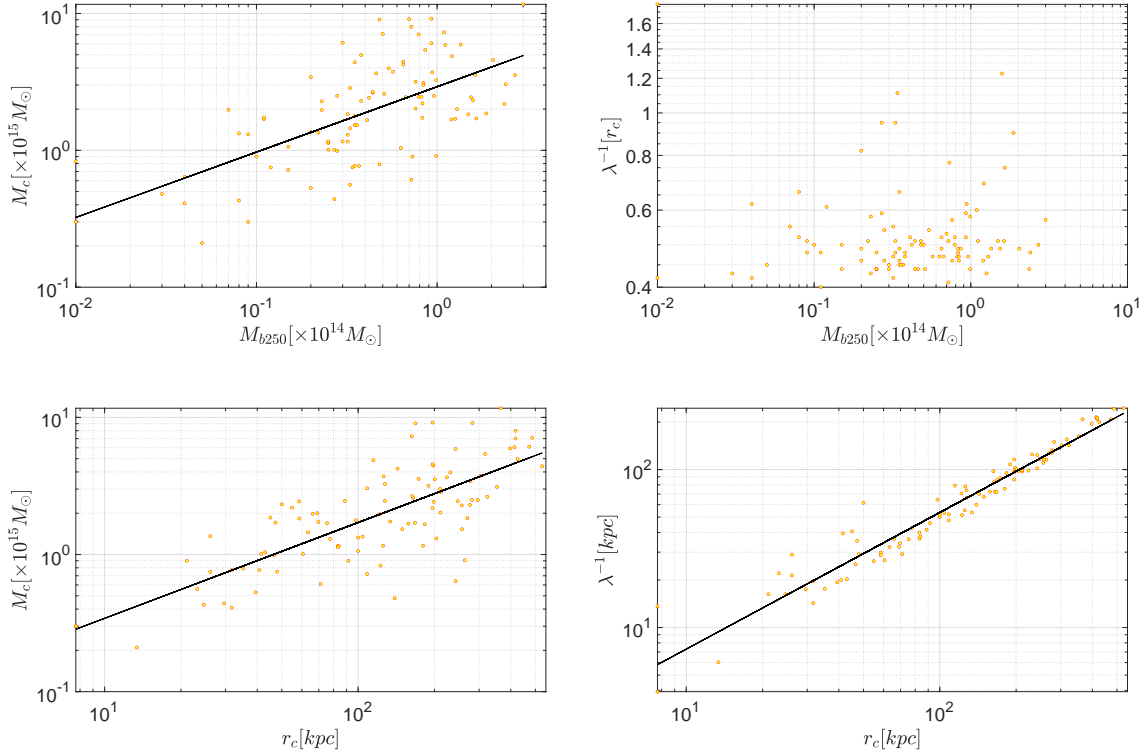


Figure 3. The plot displays M_c and λ^{-1} as functions of both M_{b250} and r_c . It is evident from the plots that there is nearly no correlation between λ^{-1} and M_{b250} . However, all the other plots reveal a robust positive correlation.

The core radius, r_c , of a cluster somehow gives its size and shape of the background matter distribution. Therefore, we can expect a strong relation between the M_c and r_c . The relation of r_c with λ^{-1} is very close to linear.

In Fig. 5, we show our results for all 106 clusters. The greenish-yellow curve shows the baryonic mass of the cluster, and the solid red curve shows the Newtonian dynamic mass. The dotted yellow ochre line shows the left-hand side of Eq. 3.12, i.e. the dynamic mass equivalent calculated from the Machian Gravity. The plots show that the masses match significantly well. We have also shown the fitting for fixed values of M_c and λ^{-1} in black dotted line. We use the median averaged value of the quantities, which gives $\lambda^{-1} = 0.4949r_c$ and $M_c = 2.759 \times 10^{15} M_\odot$. The median averaging is taken to ignore the outliers, which, if included, can significantly affect the results. We can see that even fixed values of M_c and λ^{-1} can provide a significantly good fit to the Newtonian dynamic mass of the clusters. The results from all the analyses are given in the table 1.

4.1 Fitting with three parameters

While in Fig. 5, we can see that the Machian gravity model fits the dynamic mass very well, the data indicating a power of 0.3, instead of a square root relation. Also, in the plots shown in Fig. 5, we can see that the Machian gravity gives a declining trend towards the edge of the cluster. Decreasing the power of M_b in the equation can fix this issue. Therefore, we try to relax that relation and test how we can improve the fits by relaxing the square root using a variable power, i.e.,

$$K = \left(\frac{M_c}{M_b(r)} \right)^\alpha - 1. \quad (4.6)$$

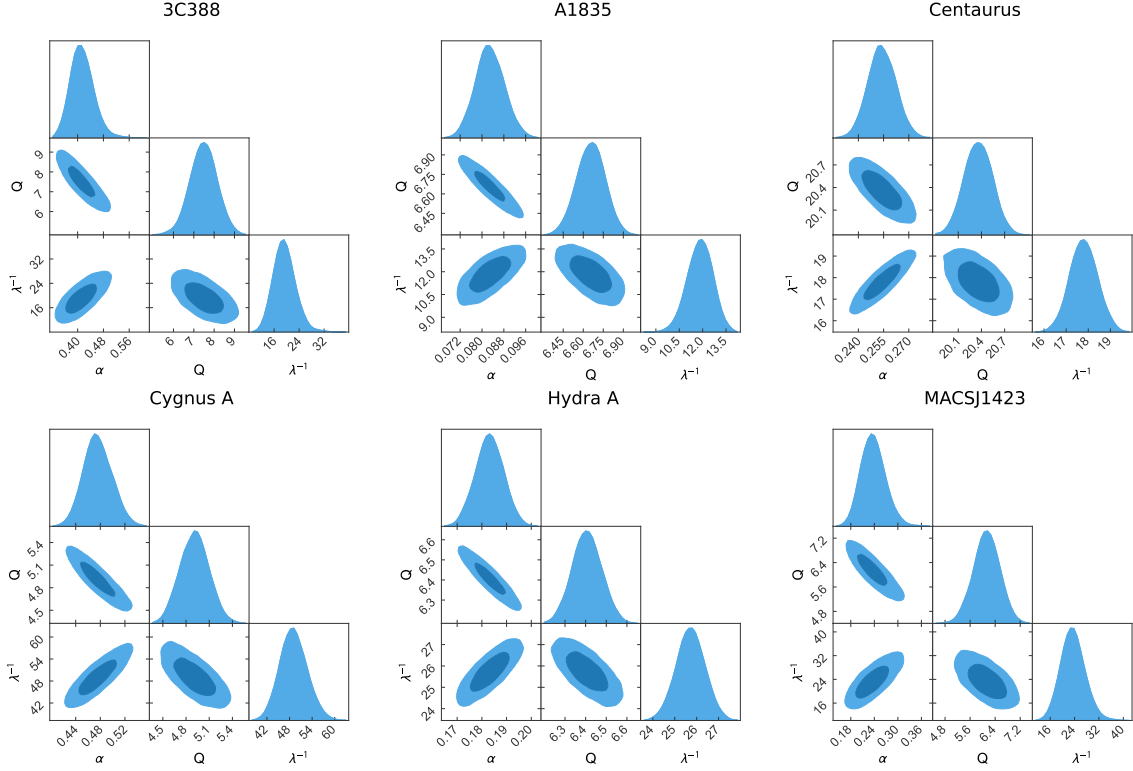


Figure 4. We’ve presented corner plots depicting a 3-parameter analysis across six galaxy clusters. In all the plots, there’s an evident negative correlation between λ^{-1} and α with respect to Q , while indicating a positive correlation between α and λ^{-1} .

However, this type of parameterization is difficult to use because α and M_c are strongly correlated and depending on the value of α , the value of the M_c can be several orders of magnitude different. Therefore, we just multiply and divide this fraction by the total mass of the galaxy and redefine the K as

$$K = \left(\frac{M_c}{M_b(r_{out})} \right)^\alpha \left(\frac{M_b(r_{out})}{M_b(r)} \right)^\alpha - 1 = Q \left(\frac{M_b(r_{out})}{M_b(r)} \right)^\alpha - 1 \quad (4.7)$$

where $Q = \left(\frac{M_c}{M_b(r_{out})} \right)^\alpha$. In this way, the factor Q will get limited by the fraction of the mass discrepancy, and the power can be varied without affecting Q . So, the effective dynamic mass from the Machian gravity can be written as

$$M_d(r) = M_b(r) \left[1 + \left(Q \left(\frac{M_b(r_{out})}{M_b(r)} \right)^\alpha - 1 \right) (1 - e^{-\lambda r} (1 + \lambda r)) \right]. \quad (4.8)$$

We can use MCMC to fit the results against the observations and constrain the Q , α , and λ^{-1} . For testing this, we use the data from [32], where they analyze the spectra for 44 galaxy clusters and calculate the dynamic mass and the gas mass of the clusters up to r_{2500} .

In Fig. 4, we have shown the corner plots for 6 of the clusters. We can see that there are strong negative correlation of Q with the other two variables, while it shows a positive correlation between the λ^{-1} and α . In Fig. 6, I have plotted the fittings for all the 44 clusters. The red curves with the errorbars are the baryonic mass of the galactic clusters. The Blue errorbars show the dynamic mass of the clusters. The fitting is shown in the orange curve. We can see that the curves fit extremely well against the observations. The fitted values of these parameters are shown in the table 2. We

can see that for all the clusters, the best fit α is coming out to be much less than 0.5, showing that for clusters, the dependence on the enclosed mass within a radius is smaller. In fact, for some of the clusters, α is even less than 0.1, showing that dynamic mass is almost independent of the enclosed mass for these clusters. Q is roughly of the order of 10. The green curves in Fig. 4 show the best-fit plots when we keep the $\alpha = 0.3$. We can see that for most of the clusters; the fitting is really good even for this fixed α , except in a few clusters, where it deviates slightly near r_{2500} .

5 Discussion and Conclusion

The Machian gravity theory introduces a modified acceleration law aimed at explaining gravity on a larger scale [23]. In our previous work, we demonstrated that this modified acceleration law effectively aligns with a broad range of spiral galaxy rotation curves, as documented in [24]. In the present study, we apply the same acceleration law to a diverse array of X-ray cluster mass profiles.

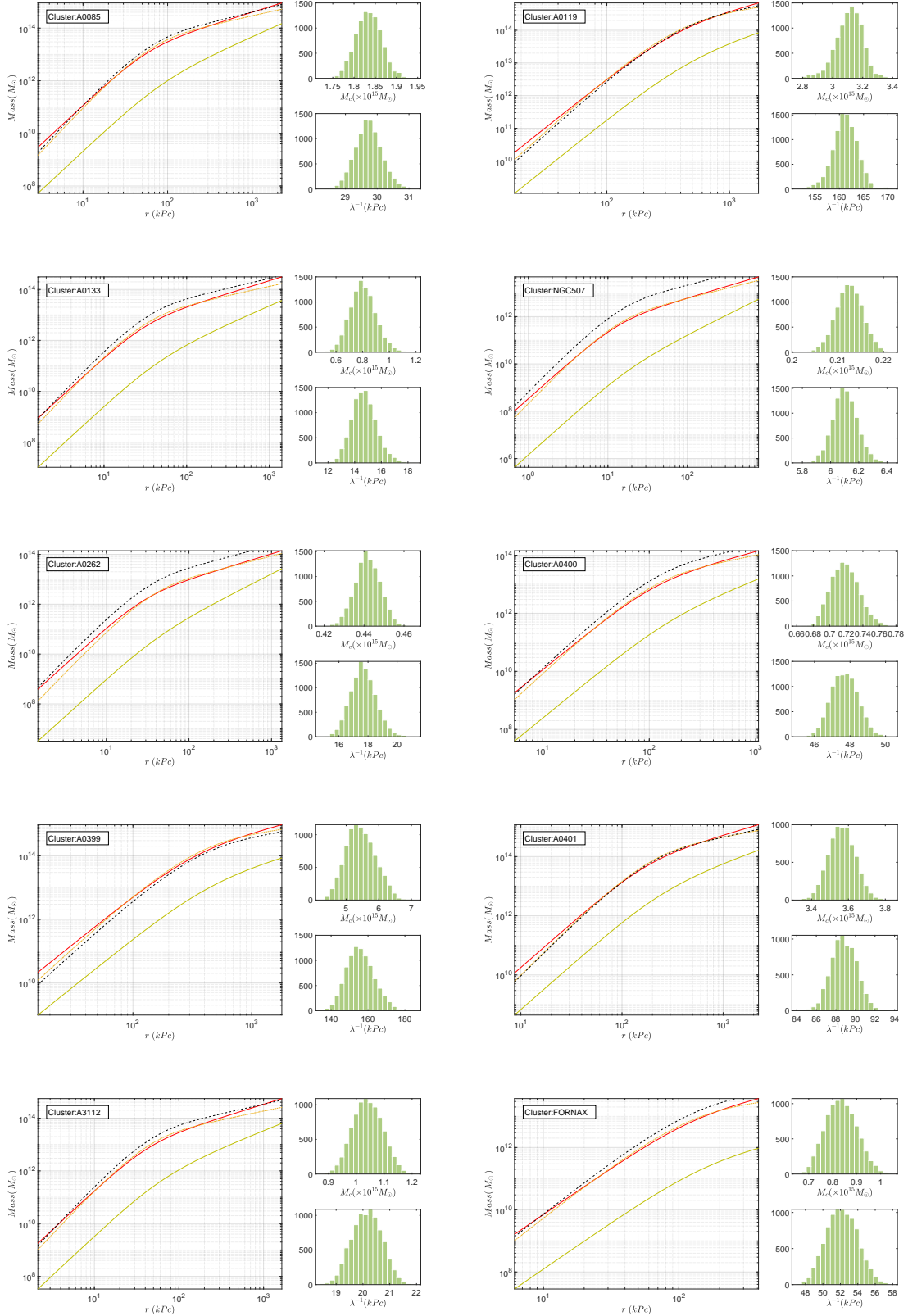
While the Modified Newtonian Dynamics (MOND) acceleration law aptly accommodates the phenomenological fitting of galaxy rotation curves, its explanatory power falters when addressing galaxy cluster mass profiles, necessitating the inclusion of supplementary dark matter components. Our findings reveal that despite the efficacy of the square root relationship for K in explaining the Tully Fisher relation for spiral galaxies, it also provides a satisfactory fit to the cluster data, even with fixed M_c and λ^{-1} . However, our analysis using cluster data indicates that a marginal alteration in the form of a power law for K significantly enhances the fitting accuracy. Given that K depends on the background mass distribution, we need a proper theory concerning the exact relation of K to determine its specific form.

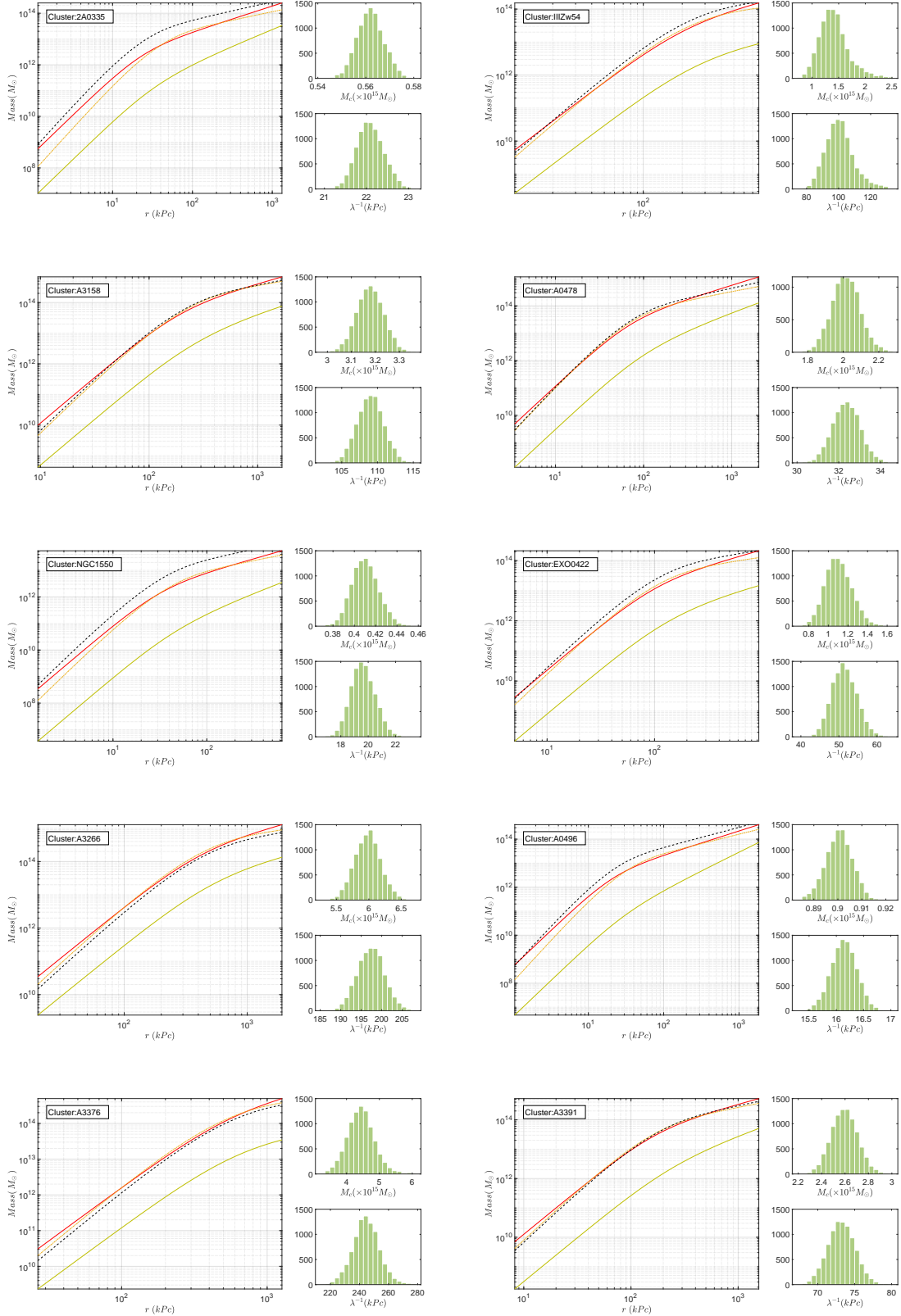
Finally, our analysis underscores a crucial revelation: for clusters, gravitational influence follows an inverse square law, contrary to theories like MOND. Therefore, the cluster analysis strongly supports the Machian Gravity theory over MOND.

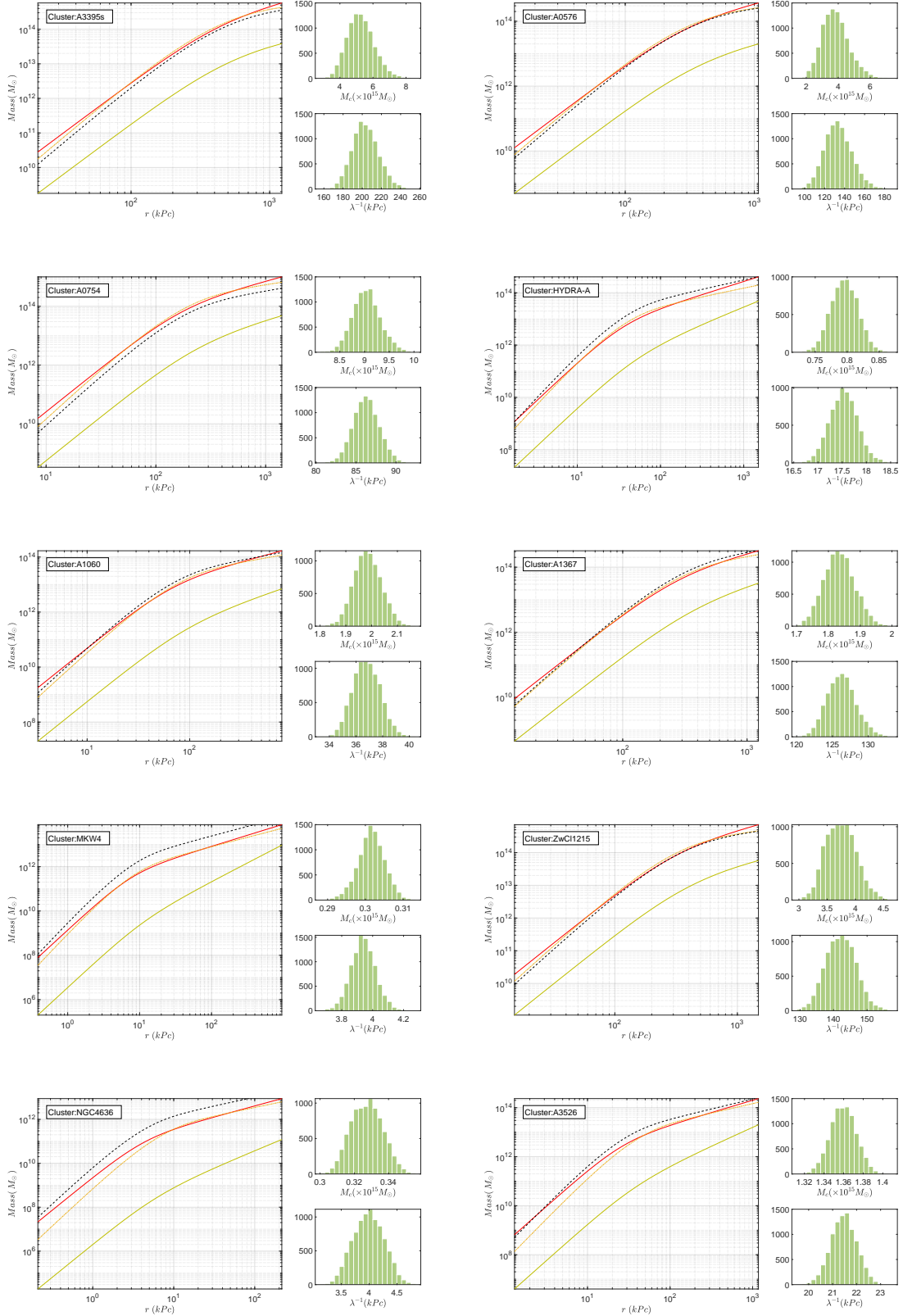
References

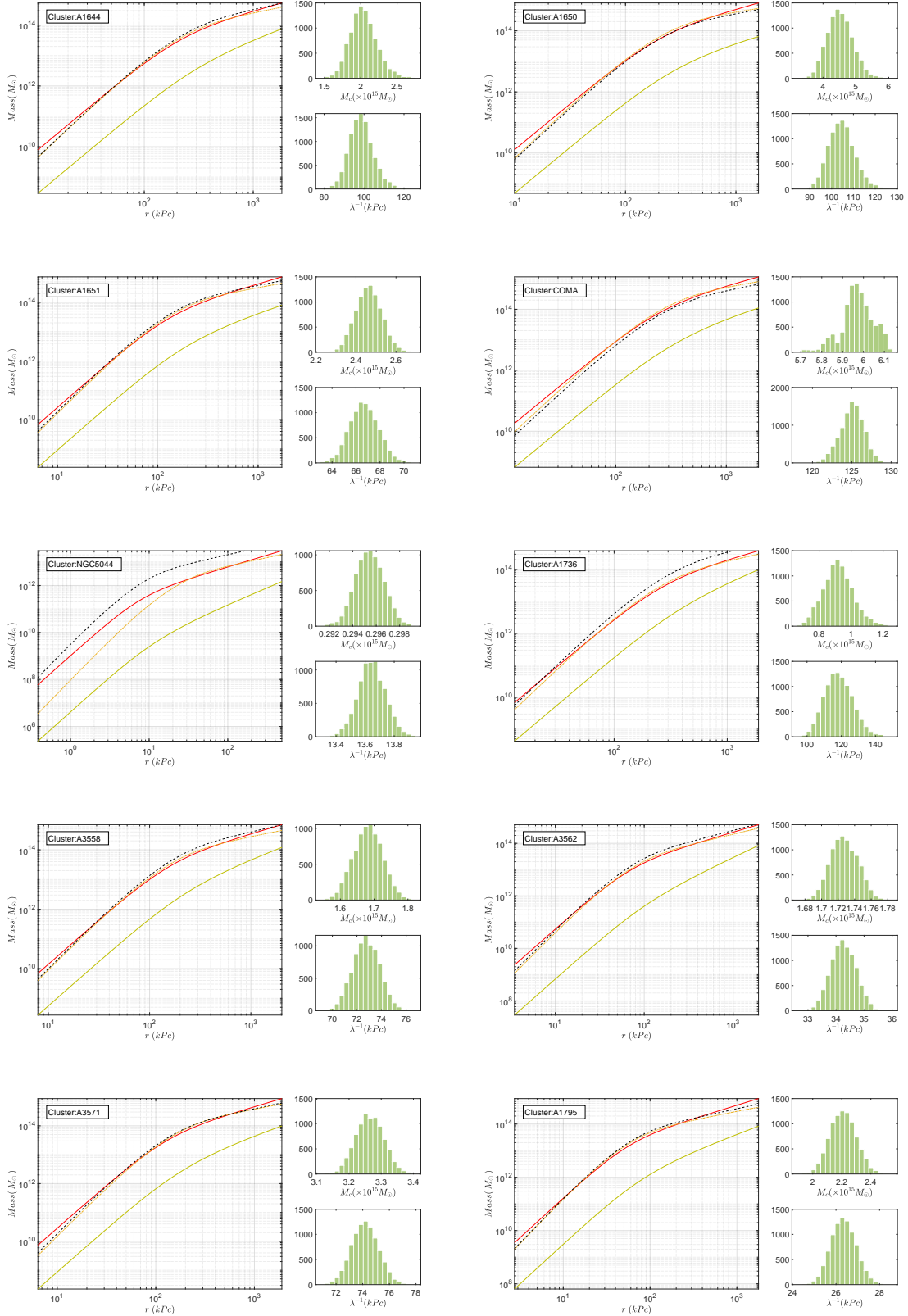
- [1] R. Sancisi, *The Visible matter - Dark matter coupling*, *IAU Symp.* **220** (2004) 233 [[astro-ph/0311348](#)].
- [2] M. Milgrom, *A Modification of the Newtonian dynamics as a possible alternative to the hidden mass hypothesis*, *Astrophys.J.* **270** (1983) 365.
- [3] M. Milgrom, *A Modification of the Newtonian dynamics: Implications for galaxies*, *Astrophys.J.* **270** (1983) 371.
- [4] M. Milgrom, *A modification of the Newtonian dynamics: implications for galaxy systems*, *Astrophys.J.* **270** (1983) 384.
- [5] M. Milgrom, *MD or DM? Modified dynamics at low accelerations vs dark matter*, *PoS HRMS2010* (2010) 033 [[1101.5122](#)].
- [6] J. Bekenstein and M. Milgrom, *Does the missing mass problem signal the breakdown of Newtonian gravity?*, *Astrophys.J.* **286** (1984) 7.
- [7] J.D. Bekenstein, *Relativistic MOND as an alternative to the dark matter paradigm*, *Nucl.Phys.* **A827** (2009) 555C [[0901.1524](#)].
- [8] M. Milgrom, *Solutions for the modified Newtonian dynamics field equation*, *Astrophys.J.* **302** (1986) 617.
- [9] J. Moffat, *Scalar-tensor-vector gravity theory*, *JCAP* **0603** (2006) 004 [[gr-qc/0506021](#)].
- [10] J. Brownstein and J. Moffat, *Galaxy rotation curves without non-baryonic dark matter*, *Astrophys.J.* **636** (2006) 721 [[astro-ph/0506370](#)].
- [11] J. Brownstein and J. Moffat, *Galaxy cluster masses without non-baryonic dark matter*, *Mon.Not.Roy.Astron.Soc.* **367** (2006) 527 [[astro-ph/0507222](#)].
- [12] J. Moffat and V. Toth, *Modified Gravity: Cosmology without dark matter or Einstein's cosmological constant*, [0710.0364](#).

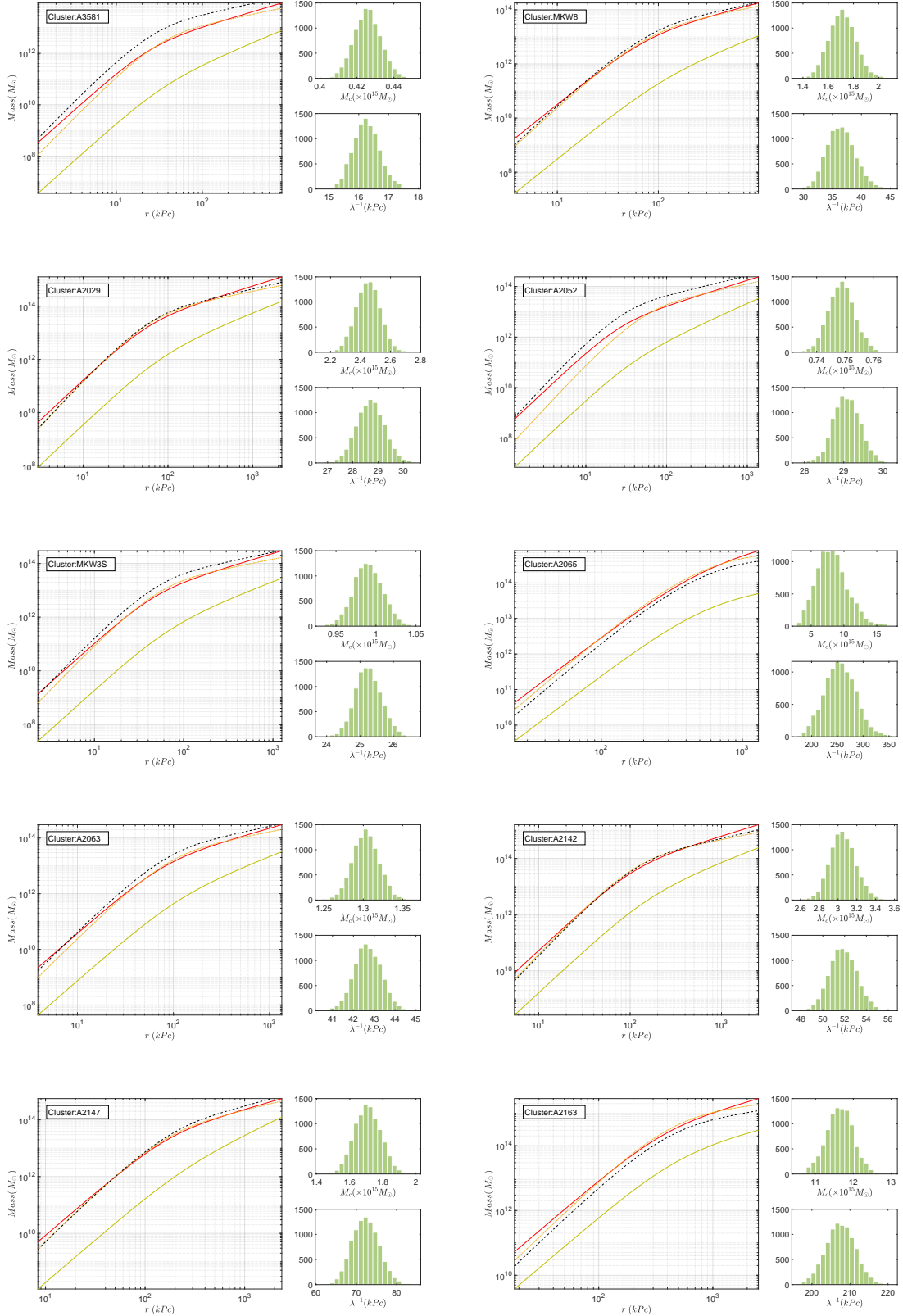
- [13] J.D. Bekenstein, *Relativistic gravitation theory for the MOND paradigm*, *Phys.Rev.* **D70** (2004) 083509 [[astro-ph/0403694](#)].
- [14] H. van Dam and M. Veltman, *Massive and massless Yang-Mills and gravitational fields*, *Nucl.Phys.* **B22** (1970) 397.
- [15] V. Zakharov, *Linearized gravitation theory and the graviton mass*, *JETP Lett.* **12** (1970) 312.
- [16] E. Babichev, C. Deffayet and R. Ziour, *The Recovery of General Relativity in massive gravity via the Vainshtein mechanism*, *Phys.Rev.* **D82** (2010) 104008 [[1007.4506](#)].
- [17] E. Babichev and M. Crisostomi, *Restoring general relativity in massive bigravity theory*, *Phys.Rev.* **D88** (2013) 084002 [[1307.3640](#)].
- [18] J. Overduin and P. Wesson, *Kaluza-Klein gravity*, *Phys.Rept.* **283** (1997) 303 [[gr-qc/9805018](#)].
- [19] J. Ponce de Leon and P.S. Wesson, *Exact solutions and the effective equation of state in Kaluza-Klein theory*, *Journal of Mathematical Physics* **34** (1993) 4080.
- [20] P.S. Wesson and J.P. de Leon, *Kaluza-Klein equations, Einstein's equations, and an effective energy-momentum tensor.*, *Journal of Mathematical Physics* **33** (1992) 3883.
- [21] J.P. de Leon, *Schwarzschild-like exteriors for stars in kaluza-klein gravity*, *arXiv preprint arXiv:1003.3151* (2010) .
- [22] P. Moraes, *Cosmic acceleration from varying masses in five dimensions*, *International Journal of Modern Physics D* **25** (2016) 1650009.
- [23] S. Das, *Aspects of machian gravity (i): A mathematical formulation for mach's principle*, 2023.
- [24] S. Das, *Aspects of machian gravity (ii): Testing theory against rotation curves of 175 sparc galaxies*, 2023.
- [25] T.H. Reiprich, *Cosmological implications and physical properties of an x-ray flux-limited sample of galaxy clusters*, 2003.
- [26] S.S. McGaugh, *A tale of two paradigms: the mutual incommensurability of λ cdm and mond*, *Canadian Journal of Physics* **93** (2015) 250.
- [27] M. Jammer, *Concepts of mass in contemporary physics and philosophy*, Princeton Univ. Press (2000).
- [28] J. Moffat and V. Toth, *Fundamental parameter-free solutions in modified gravity*, *Class.Quant.Grav.* **26** (2009) 085002 [[0712.1796](#)].
- [29] I.R. King, *The structure of star clusters. IV. Photoelectric surface photometry in nine globular clusters*, *Astronomical Journal* **71** (1966) 276.
- [30] A. Cavaliere and R. Fusco-Femiano, *X-rays from hot plasma in clusters of galaxies*, *Astronomy and Astrophysics* **49** (1976) 137.
- [31] R. Sanders, *A faber-jackson relation for clusters of galaxies: Implications for modified dynamics*, *Astronomy and Astrophysics* **284** (1994) L31.
- [32] R. Main, B. McNamara, P. Nulsen, H. Russell and A. Vantyghem, *A relationship between halo mass, cooling, agn heating, and the coevolution of massive black holes*, *Monthly Notices of the Royal Astronomical Society* (2016) stw2644.

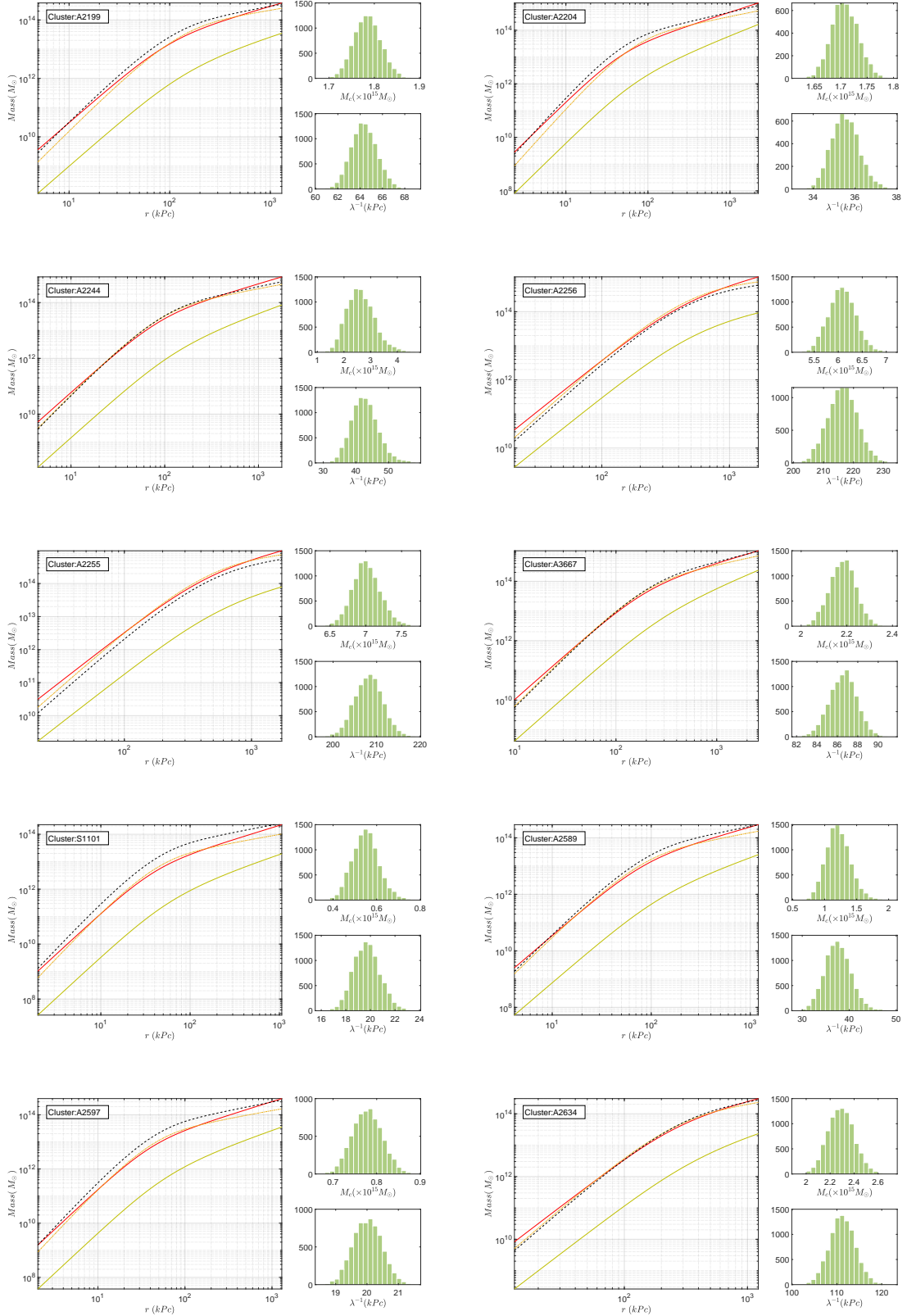


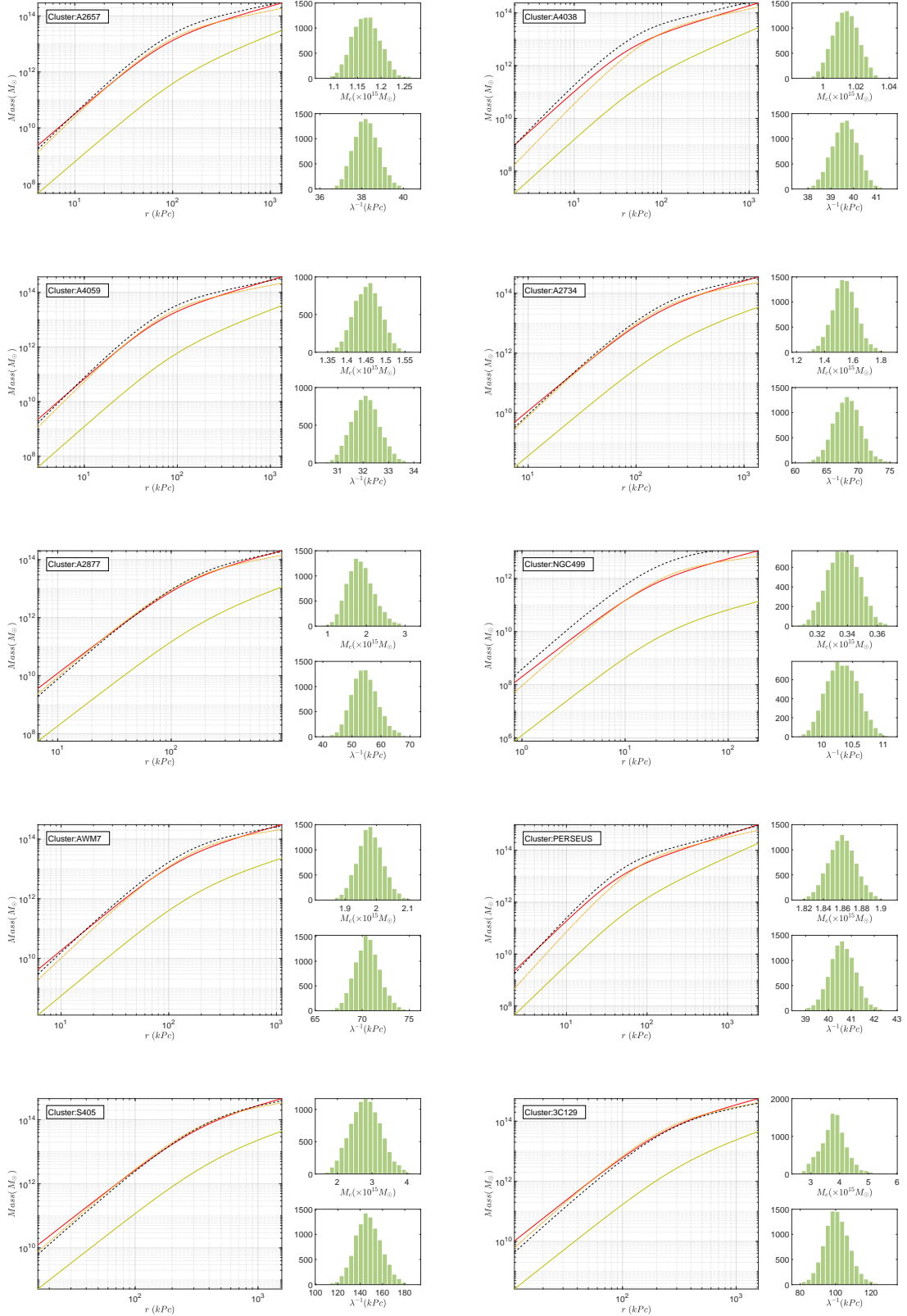


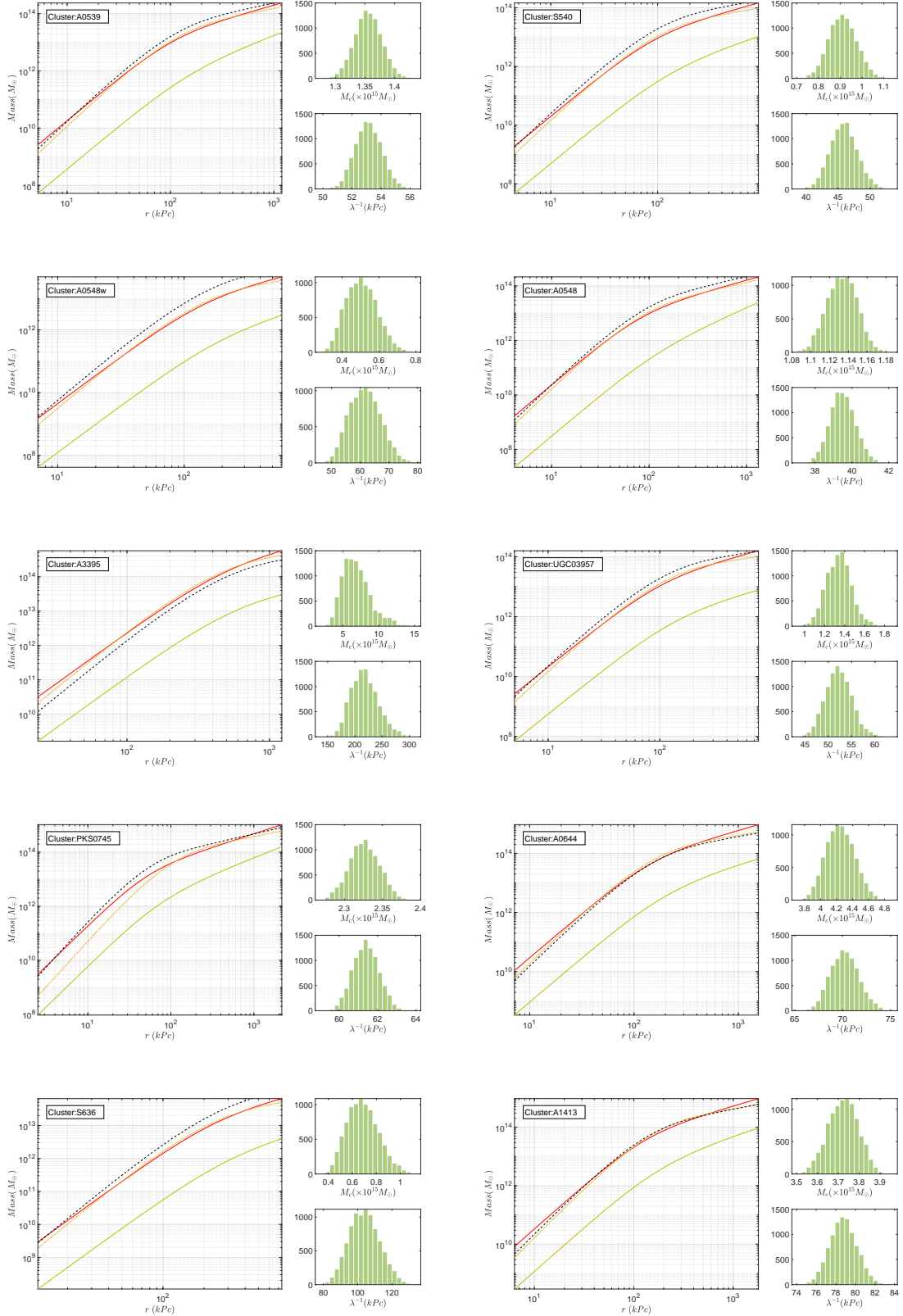


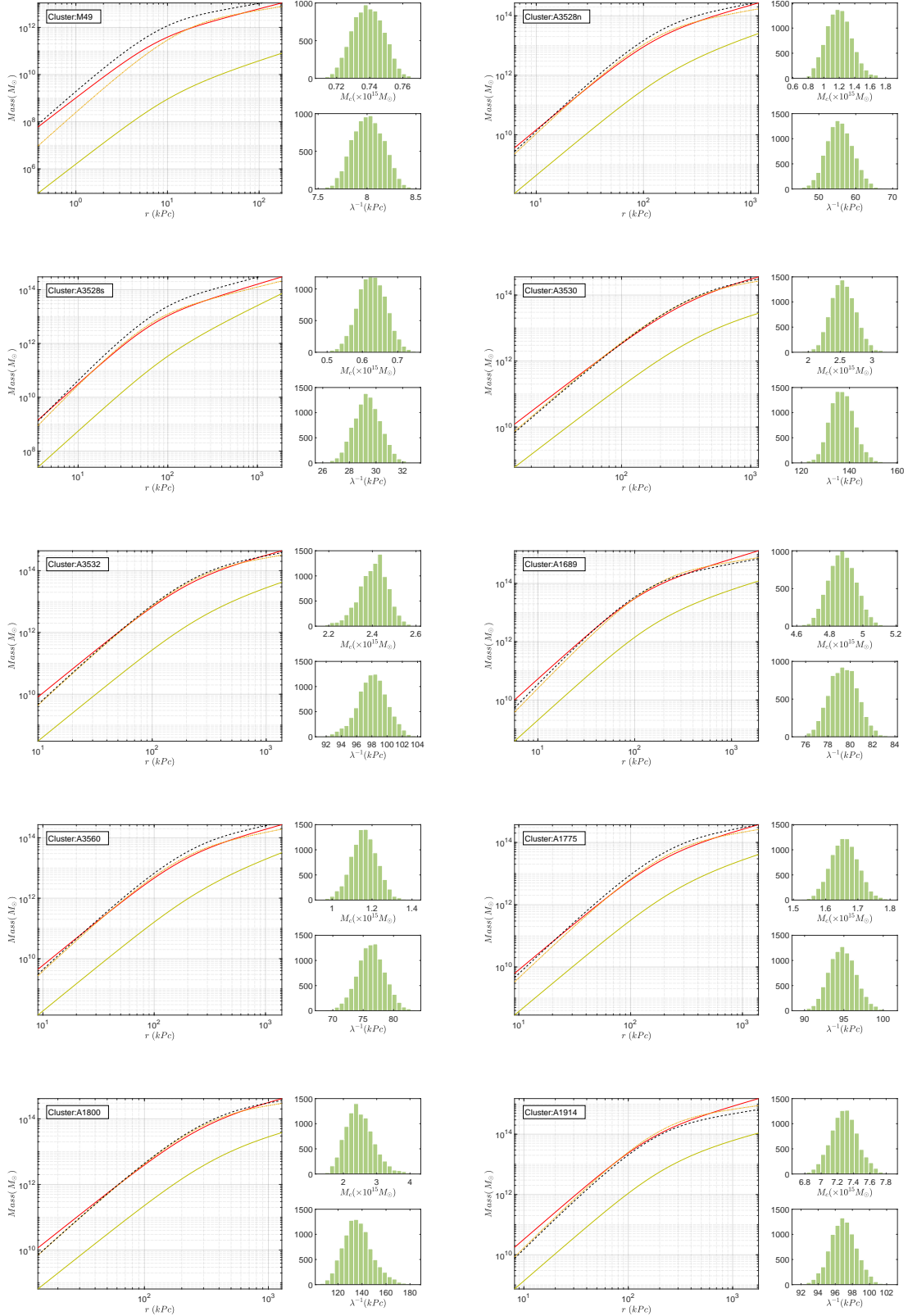


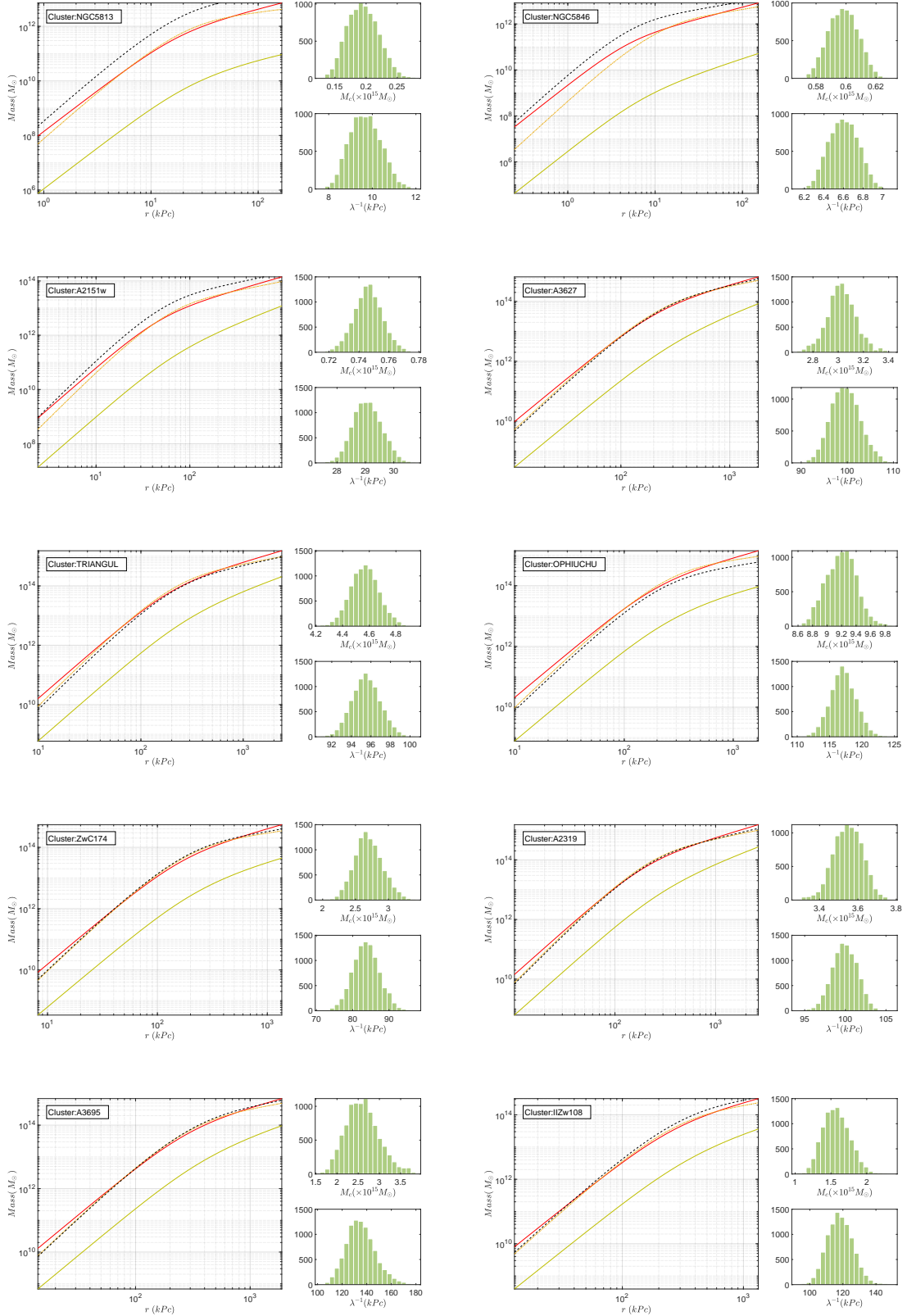












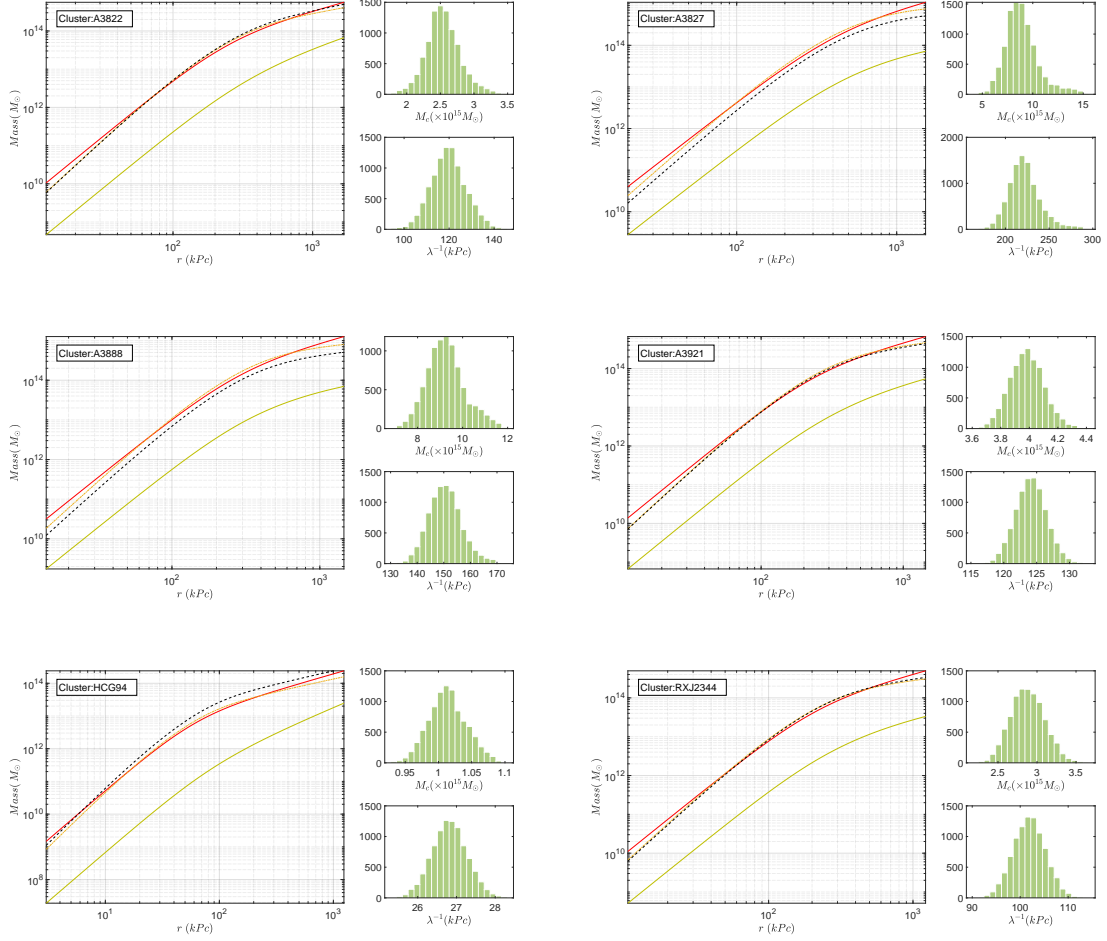
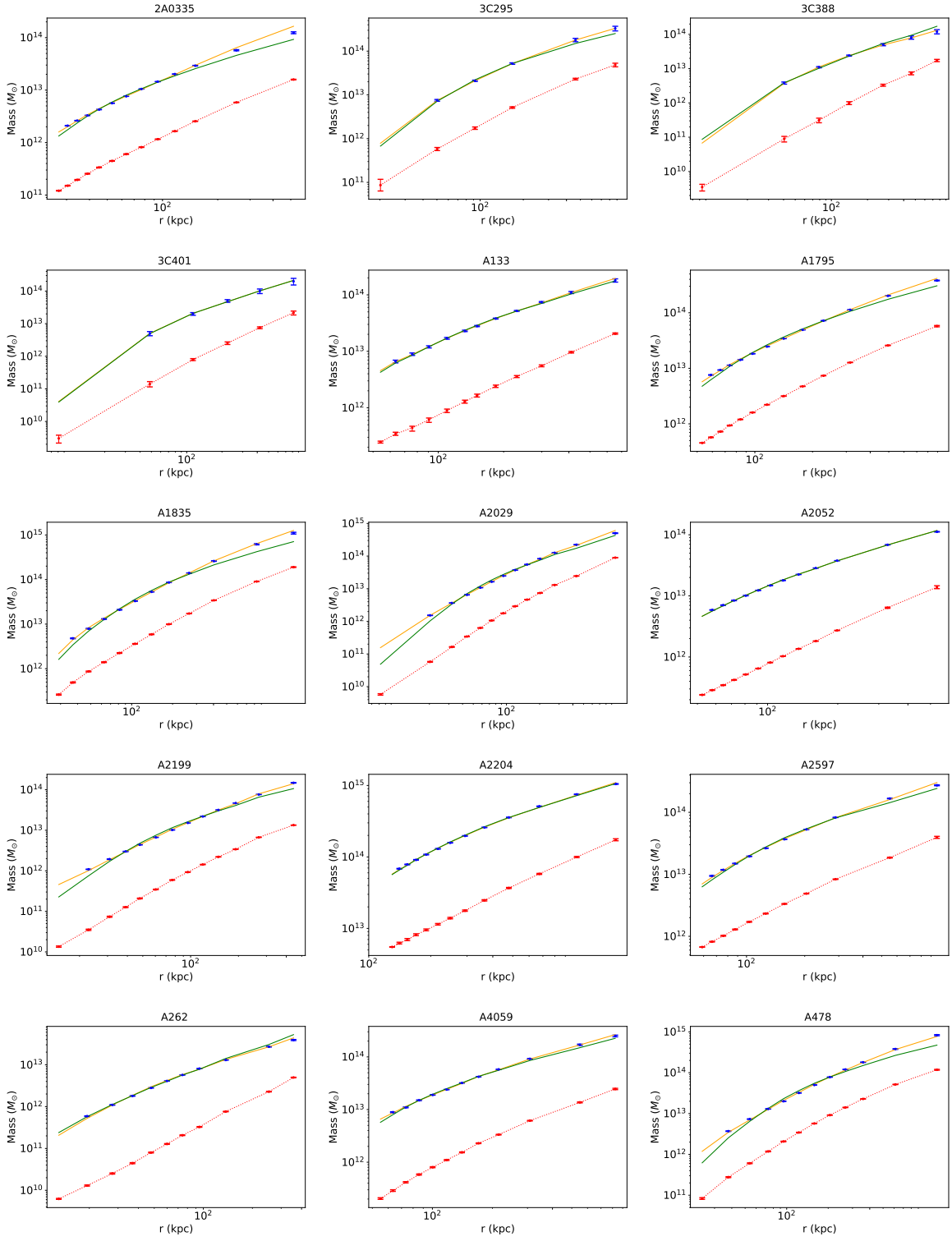
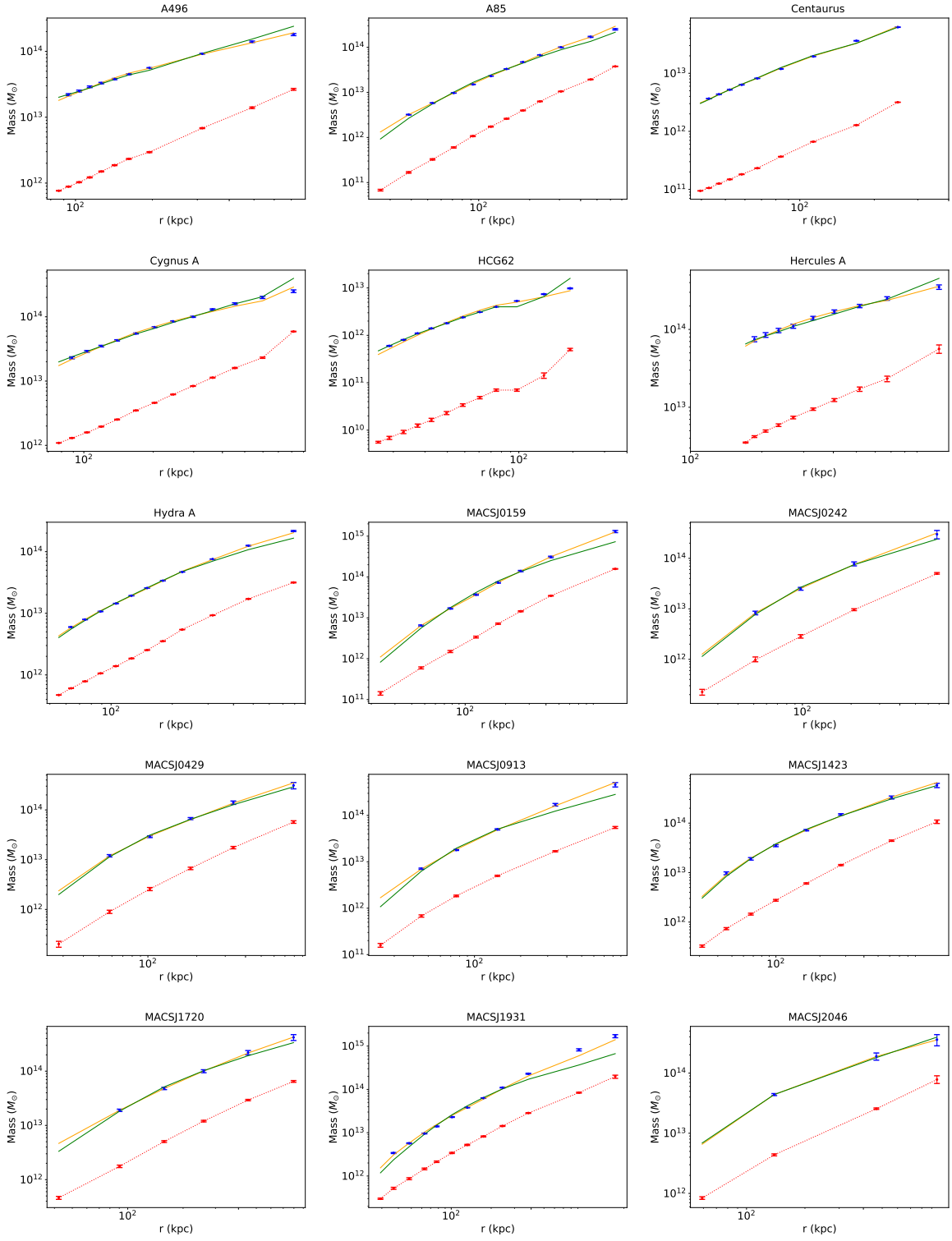


Figure 5. The radial mass profiles of different galaxy clusters are shown here. The solid yellow line shows the physical mass of the galaxy cluster, calculated using King β model. The dotted cyan line shows the dynamic mass of the galaxy cluster calculated given by the Newtonian mechanics using Eq. 3.11, and the dotted red line shows the dynamic mass equivalent of the galaxy cluster given by the theory proposed in this paper i.e. using Eq. 3.12. The plots show that the dynamic mass equivalent from the present theory matches well with the Newtonian dynamic mass of the cluster, eliminating the requirement of having any exotic dark matter in the clusters.





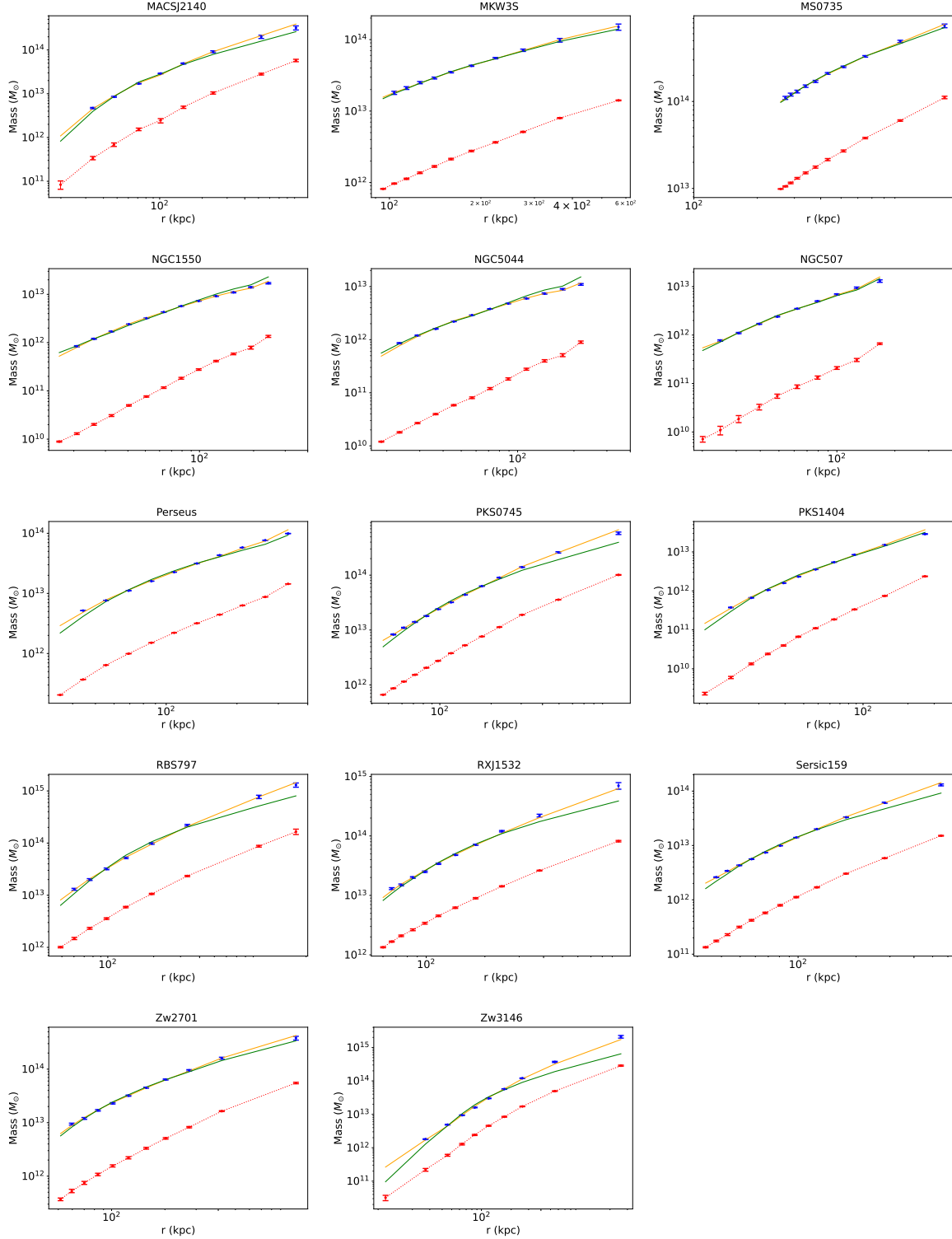


Figure 6. The radial mass profiles of various galaxy clusters are presented in this illustration. The red error bars, depicted with a dotted line, represent the physical mass of each galaxy cluster. The blue error bars indicate the Newtonian dynamic mass of the clusters. The orange line represents the best-fit line for the dynamic mass equivalent of the galaxy cluster, derived from Eq. 4.8. Additionally, a green curve displays the best fit obtained when α is set to 0.3. The best-fit line for the dynamic mass equivalent, derived from Machian Gravity theory, solely based on the cluster’s physical gas mass, eliminates the necessity for any exotic dark matter within the clusters.

Cluster	T [keV]	ρ_0 $\times 10^{-25}$ [g/cm ³]	β	r_c [kpc]	r_{250} [kpc]	M_{b250} $\times 10^{14}$ [M_\odot]	M_{d250} $\times 10^{14}$ [M_\odot]	M_c $\times 10^{15}$ [M_\odot]	λ^{-1} [r_c]
A0085	6.90 ^{0.40} _{-0.40}	0.34	0.532 ^{0.004} _{-0.004}	58.5 ^{3.3} _{-3.9}	2241.0 ^{139.0} _{-162.0}	1.49	9.02 ^{0.53} _{-0.53}	1.83 ^{0.05} _{-0.02}	0.51 ^{0.005} _{-0.004}
A0119	5.60 ^{0.30} _{-0.30}	0.03	0.675 ^{0.026} _{-0.023}	352.8 ^{24.7} _{-27.0}	1728.0 ^{156.0} _{-173.0}	0.84	6.88 ^{0.46} _{-0.44}	3.11 ^{0.06} _{-0.06}	0.46 ^{0.005} _{-0.005}
A0133	3.80 ^{2.00} _{-0.90}	0.42	0.530 ^{0.004} _{-0.004}	31.7 ^{1.9} _{-2.3}	1417.0 ^{96.0} _{-109.0}	0.37	3.13 ^{1.65} _{-0.74}	0.77 ^{0.09} _{-0.05}	0.45 ^{0.020} _{-0.016}
NGC507	1.26 ^{0.07} _{-0.07}	0.23	0.444 ^{0.005} _{-0.005}	13.4 ^{0.9} _{-1.0}	783.0 ^{64.0} _{-70.0}	0.05	0.48 ^{0.03} _{-0.03}	0.21 ^{0.08} _{-0.00}	0.45 ^{0.004} _{-0.004}
A0262	2.15 ^{0.06} _{-0.06}	0.16	0.443 ^{0.018} _{-0.017}	29.6 ^{8.5} _{-7.2}	1334.0 ^{432.0} _{-386.0}	0.27	1.39 ^{0.07} _{-0.07}	0.44 ^{0.07} _{-0.00}	0.59 ^{0.020} _{-0.017}
A0400	2.31 ^{0.14} _{-0.14}	0.04	0.534 ^{0.014} _{-0.013}	108.5 ^{7.8} _{-8.8}	1062.0 ^{97.0} _{-108.0}	0.15	1.42 ^{0.09} _{-0.09}	0.72 ^{0.07} _{-0.01}	0.44 ^{0.004} _{-0.004}
A0399	7.00 ^{0.40} _{-0.40}	0.04	0.713 ^{0.137} _{-0.095}	316.9 ^{93.9} _{-72.7}	1791.0 ^{683.0} _{-744.0}	0.86	9.51 ^{1.91} _{-1.39}	5.41 ^{0.30} _{-0.24}	0.49 ^{0.016} _{-0.013}
A0401	8.00 ^{0.40} _{-0.40}	0.11	0.613 ^{0.010} _{-0.010}	173.2 ^{10.7} _{-12.0}	2236.0 ^{167.0} _{-182.0}	1.63	11.96 ^{0.63} _{-0.63}	3.56 ^{0.05} _{-0.04}	0.51 ^{0.005} _{-0.004}
A3112	5.30 ^{0.70} _{-1.00}	0.54	0.576 ^{0.006} _{-0.006}	43.0 ^{2.8} _{-3.2}	1644.0 ^{124.0} _{-138.0}	0.63	5.50 ^{0.73} _{-1.04}	1.04 ^{0.07} _{-0.03}	0.47 ^{0.008} _{-0.007}
FORNAX	1.20 ^{0.04} _{-0.04}	0.02	0.804 ^{0.098} _{-0.084}	122.5 ^{13.0} _{-12.6}	387.0 ^{67.0} _{-74.0}	0.01	0.37 ^{0.05} _{-0.04}	0.83 ^{0.08} _{-0.04}	0.42 ^{0.009} _{-0.008}
2A0335	3.01 ^{0.07} _{-0.07}	1.07	0.575 ^{0.004} _{-0.003}	23.2 ^{1.2} _{-1.5}	1322.0 ^{74.0} _{-92.0}	0.33	2.51 ^{0.06} _{-0.06}	0.56 ^{0.07} _{-0.00}	0.95 ^{0.009} _{-0.010}
IIIZw54	2.16 ^{0.35} _{-0.30}	0.04	0.887 ^{0.320} _{-0.151}	203.5 ^{87.7} _{-52.7}	780.0 ^{389.0} _{-461.0}	0.09	1.54 ^{0.61} _{-0.35}	1.31 ^{0.22} _{-0.14}	0.48 ^{0.031} _{-0.023}
A3158	5.77 ^{0.10} _{-0.05}	0.08	0.661 ^{0.025} _{-0.022}	189.4 ^{16.2} _{-17.1}	1672.0 ^{189.0} _{-206.0}	0.76	6.91 ^{0.29} _{-0.24}	3.17 ^{0.05} _{-0.03}	0.57 ^{0.006} _{-0.006}
A0478	8.40 ^{0.80} _{-1.40}	0.50	0.613 ^{0.004} _{-0.004}	69.0 ^{3.2} _{-4.1}	2029.0 ^{105.0} _{-130.0}	1.29	11.45 ^{1.09} _{-1.91}	2.00 ^{0.07} _{-0.05}	0.47 ^{0.006} _{-0.006}
NGC1550	1.43 ^{0.04} _{-0.03}	0.15	0.554 ^{0.049} _{-0.037}	31.7 ^{10.6} _{-7.9}	632.0 ^{247.0} _{-231.0}	0.04	0.55 ^{0.05} _{-0.04}	0.41 ^{0.07} _{-0.01}	0.62 ^{0.018} _{-0.016}
EX00422	2.90 ^{0.90} _{-0.60}	0.13	0.722 ^{0.104} _{-0.071}	100.0 ^{28.5} _{-21.9}	934.0 ^{338.0} _{-367.0}	0.15	2.12 ^{0.73} _{-0.49}	1.06 ^{0.11} _{-0.08}	0.50 ^{0.021} _{-0.019}
A3266	8.00 ^{0.50} _{-0.50}	0.05	0.796 ^{0.020} _{-0.019}	397.2 ^{22.4} _{-26.4}	1915.0 ^{132.0} _{-150.0}	1.35	12.83 ^{0.87} _{-0.86}	5.93 ^{0.12} _{-0.12}	0.49 ^{0.005} _{-0.005}
A0496	4.13 ^{0.08} _{-0.08}	0.65	0.484 ^{0.003} _{-0.003}	21.1 ^{1.1} _{-1.4}	1830.0 ^{111.0} _{-130.0}	0.73	4.01 ^{0.08} _{-0.08}	0.90 ^{0.06} _{-0.00}	0.77 ^{0.007} _{-0.008}
A3376	4.00 ^{0.40} _{-0.40}	0.02	1.054 ^{0.101} _{-0.083}	531.7 ^{53.5} _{-51.8}	1264.0 ^{169.0} _{-183.0}	0.35	4.97 ^{0.70} _{-0.65}	4.40 ^{0.28} _{-0.24}	0.46 ^{0.011} _{-0.011}
A3391	5.40 ^{0.60} _{-0.60}	0.05	0.579 ^{0.026} _{-0.024}	164.8 ^{18.3} _{-18.1}	1558.0 ^{227.0} _{-234.0}	0.51	5.29 ^{0.63} _{-0.63}	2.59 ^{0.08} _{-0.07}	0.44 ^{0.007} _{-0.007}
A3395s	5.00 ^{0.30} _{-0.30}	0.03	0.964 ^{0.275} _{-0.167}	425.4 ^{123.1} _{-86.5}	1223.0 ^{442.0} _{-501.0}	0.38	5.77 ^{1.70} _{-1.12}	4.97 ^{0.56} _{-0.44}	0.47 ^{0.021} _{-0.018}
A0576	4.02 ^{0.07} _{-0.07}	0.03	0.825 ^{0.432} _{-0.185}	277.5 ^{156.1} _{-89.4}	1066.0 ^{703.0} _{-903.0}	0.20	3.67 ^{1.93} _{-0.86}	3.43 ^{0.64} _{-0.44}	0.46 ^{0.035} _{-0.028}
A0754	9.50 ^{0.70} _{-0.40}	0.09	0.698 ^{0.027} _{-0.024}	168.3 ^{13.9} _{-14.7}	1402.0 ^{156.0} _{-170.0}	0.48	10.06 ^{0.84} _{-0.55}	9.04 ^{0.19} _{-0.17}	0.51 ^{0.006} _{-0.006}
HYDRA-A	4.30 ^{0.40} _{-0.40}	0.63	0.573 ^{0.003} _{-0.003}	35.2 ^{1.6} _{-2.1}	1502.0 ^{76.0} _{-95.0}	0.48	4.06 ^{0.38} _{-0.38}	0.79 ^{0.07} _{-0.01}	0.50 ^{0.005} _{-0.005}
A1060	3.24 ^{0.06} _{-0.06}	0.09	0.607 ^{0.040} _{-0.034}	66.2 ^{10.9} _{-9.9}	790.0 ^{171.0} _{-176.0}	0.07	1.69 ^{0.12} _{-0.10}	1.98 ^{0.06} _{-0.03}	0.55 ^{0.009} _{-0.009}
A1367	3.55 ^{0.08} _{-0.08}	0.03	0.695 ^{0.035} _{-0.032}	269.7 ^{20.4} _{-21.7}	1234.0 ^{131.0} _{-141.0}	0.32	3.19 ^{0.18} _{-0.16}	1.84 ^{0.06} _{-0.03}	0.47 ^{0.005} _{-0.004}
MKW4	1.71 ^{0.09} _{-0.09}	0.57	0.440 ^{0.004} _{-0.005}	7.7 ^{0.8} _{-0.8}	948.0 ^{108.0} _{-110.0}	0.09	0.78 ^{0.04} _{-0.04}	0.30 ^{0.07} _{-0.00}	0.51 ^{0.007} _{-0.006}
ZwCl1215	5.58 ^{0.89} _{-0.78}	0.05	0.819 ^{0.038} _{-0.034}	303.5 ^{23.5} _{-24.5}	1485.0 ^{155.0} _{-167.0}	0.57	7.15 ^{1.19} _{-1.04}	3.75 ^{0.19} _{-0.15}	0.47 ^{0.010} _{-0.009}
NGC4636	0.76 ^{0.01} _{-0.01}	0.33	0.491 ^{0.032} _{-0.027}	4.2 ^{2.1} _{-1.4}	216.0 ^{118.0} _{-92.0}	0.00	0.09 ^{0.01} _{-0.00}	0.33 ^{0.07} _{-0.01}	0.95 ^{0.038} _{-0.038}
A3526	3.68 ^{0.06} _{-0.06}	0.29	0.495 ^{0.011} _{-0.010}	26.1 ^{3.7} _{-3.2}	1175.0 ^{189.0} _{-174.0}	0.20	2.35 ^{0.06} _{-0.06}	1.36 ^{0.06} _{-0.01}	0.82 ^{0.012} _{-0.013}

Cluster	T [keV]	ρ_0 $\times 10^{-25}$ [g/cm ³]	β	r_c [kpc]	r_{250} [kpc]	M_{b250} $\times 10^{14}$ [M_\odot]	M_{d250} $\times 10^{14}$ [M_\odot]	M_c $\times 10^{15}$ [M_\odot]	λ^{-1} [r_c]
A1644	4.70 ^{0.90} _{-0.70}	0.04	0.579 ^{0.111} _{-0.074}	211.3 ^{90.6} _{-65.9}	1830.0 ^{937.0} _{-958.0}	0.76	5.39 ^{1.46} _{-1.06}	2.02 ^{0.14} _{-0.10}	0.46 ^{0.021} _{-0.016}
A1650	6.70 ^{0.80} _{-0.80}	0.08	0.704 ^{0.131} _{-0.081}	197.9 ^{73.7} _{-51.2}	1600.0 ^{714.0} _{-758.0}	0.65	8.16 ^{1.80} _{-1.36}	4.45 ^{0.26} _{-0.22}	0.52 ^{0.020} _{-0.017}
A1651	6.10 ^{0.40} _{-0.40}	0.15	0.643 ^{0.014} _{-0.013}	127.5 ^{8.9} _{-10.1}	1725.0 ^{151.0} _{-168.0}	0.79	7.38 ^{0.51} _{-0.51}	2.46 ^{0.06} _{-0.04}	0.52 ^{0.006} _{-0.005}
COMA	8.38 ^{0.34} _{-0.34}	0.06	0.654 ^{0.019} _{-0.021}	242.3 ^{18.6} _{-20.1}	1954.0 ^{201.0} _{-202.0}	1.11	11.57 ^{0.58} _{-0.60}	5.88 ^{0.04} _{-0.06}	0.51 ^{0.004} _{-0.004}
NGC5044	1.07 ^{0.01} _{-0.01}	0.67	0.524 ^{0.002} _{-0.003}	7.7 ^{0.8} _{-0.8}	487.0 ^{50.0} _{-53.0}	0.01	0.30 ^{0.00} _{-0.00}	0.30 ^{0.09} _{-0.00}	1.77 ^{0.008} _{-0.020}
A1736	3.50 ^{0.40} _{-0.40}	0.03	0.542 ^{0.147} _{-0.092}	263.4 ^{125.8} _{-92.7}	1889.0 ^{1110.0} _{-1229.0}	0.99	3.86 ^{1.14} _{-0.79}	0.91 ^{0.09} _{-0.05}	0.44 ^{0.020} _{-0.017}
A3558	5.50 ^{0.40} _{-0.40}	0.09	0.580 ^{0.006} _{-0.005}	157.7 ^{7.5} _{-9.6}	2021.0 ^{106.0} _{-134.0}	1.20	7.03 ^{0.52} _{-0.51}	1.68 ^{0.06} _{-0.03}	0.46 ^{0.004} _{-0.004}
A3562	5.16 ^{0.16} _{-0.16}	0.11	0.472 ^{0.006} _{-0.006}	69.7 ^{4.6} _{-5.3}	1926.0 ^{151.0} _{-167.0}	0.83	5.14 ^{0.17} _{-0.17}	1.73 ^{0.05} _{-0.01}	0.49 ^{0.004} _{-0.004}
A3571	6.90 ^{0.20} _{-0.20}	0.14	0.613 ^{0.010} _{-0.010}	127.5 ^{7.3} _{-8.7}	1897.0 ^{137.0} _{-154.0}	0.99	8.76 ^{0.29} _{-0.29}	3.26 ^{0.04} _{-0.03}	0.58 ^{0.005} _{-0.005}
A1795	7.80 ^{1.00} _{-1.00}	0.50	0.596 ^{0.003} _{-0.002}	54.9 ^{2.4} _{-3.2}	1773.0 ^{81.0} _{-106.0}	0.83	9.03 ^{1.16} _{-1.16}	2.20 ^{0.07} _{-0.05}	0.48 ^{0.006} _{-0.006}
A3581	1.83 ^{0.04} _{-0.04}	0.31	0.543 ^{0.024} _{-0.022}	24.6 ^{3.7} _{-3.1}	840.0 ^{174.0} _{-169.0}	0.08	0.92 ^{0.05} _{-0.04}	0.43 ^{0.07} _{-0.00}	0.66 ^{0.012} _{-0.011}
MKW8	3.29 ^{0.23} _{-0.22}	0.05	0.511 ^{0.098} _{-0.059}	75.4 ^{49.4} _{-29.9}	977.0 ^{703.0} _{-619.0}	0.11	1.79 ^{0.37} _{-0.24}	1.69 ^{0.08} _{-0.06}	0.48 ^{0.021} _{-0.018}
A2029	9.10 ^{1.00} _{-1.00}	0.56	0.582 ^{0.004} _{-0.004}	58.5 ^{2.8} _{-3.6}	2200.0 ^{120.0} _{-146.0}	1.54	12.77 ^{1.41} _{-1.41}	2.44 ^{0.06} _{-0.05}	0.49 ^{0.006} _{-0.006}
A2052	3.03 ^{0.04} _{-0.04}	0.52	0.526 ^{0.005} _{-0.005}	26.1 ^{1.8} _{-2.0}	1373.0 ^{106.0} _{-119.0}	0.34	2.40 ^{0.04} _{-0.04}	0.75 ^{0.07} _{-0.00}	1.11 ^{0.008} _{-0.012}
MKW3S	3.70 ^{0.20} _{-0.20}	0.31	0.581 ^{0.008} _{-0.007}	46.5 ^{2.9} _{-3.4}	1257.0 ^{93.0} _{-108.0}	0.28	2.96 ^{0.17} _{-0.16}	0.99 ^{0.06} _{-0.01}	0.54 ^{0.005} _{-0.005}
A2065	5.50 ^{0.40} _{-0.40}	0.04	1.162 ^{0.734} _{-0.282}	485.9 ^{254.4} _{-133.8}	1302.0 ^{780.0} _{-1048.0}	0.50	8.01 ^{5.12} _{-2.27}	7.10 ^{1.80} _{-1.24}	0.50 ^{0.042} _{-0.036}
A2063	3.68 ^{0.11} _{-0.11}	0.12	0.561 ^{0.011} _{-0.011}	77.5 ^{5.9} _{-6.1}	1343.0 ^{127.0} _{-130.0}	0.32	3.03 ^{0.11} _{-0.11}	1.30 ^{0.06} _{-0.01}	0.55 ^{0.005} _{-0.005}
A2142	9.70 ^{1.50} _{-1.10}	0.27	0.591 ^{0.006} _{-0.006}	108.5 ^{6.2} _{-7.4}	2537.0 ^{167.0} _{-192.0}	2.40	15.93 ^{2.47} _{-1.81}	3.04 ^{0.09} _{-0.08}	0.48 ^{0.007} _{-0.007}
A2147	4.91 ^{0.28} _{-0.28}	0.03	0.444 ^{0.071} _{-0.046}	167.6 ^{72.9} _{-46.7}	2360.0 ^{1215.0} _{-1201.0}	1.26	5.62 ^{0.95} _{-0.66}	1.70 ^{0.07} _{-0.05}	0.43 ^{0.012} _{-0.011}
A2163	13.29 ^{0.64} _{-0.64}	0.10	0.796 ^{0.030} _{-0.028}	365.5 ^{26.7} _{-29.0}	2509.0 ^{253.0} _{-273.0}	3.00	28.52 ^{1.75} _{-1.70}	11.66 ^{0.22} _{-0.28}	0.57 ^{0.006} _{-0.007}
A2199	4.10 ^{0.08} _{-0.08}	0.16	0.655 ^{0.019} _{-0.021}	97.9 ^{8.2} _{-8.9}	1300.0 ^{153.0} _{-154.0}	0.35	3.81 ^{0.13} _{-0.14}	1.78 ^{0.05} _{-0.02}	0.66 ^{0.007} _{-0.007}
A2204	7.21 ^{0.25} _{-0.25}	0.99	0.597 ^{0.008} _{-0.007}	47.2 ^{2.9} _{-3.4}	2216.0 ^{169.0} _{-196.0}	1.65	10.46 ^{0.39} _{-0.38}	1.71 ^{0.06} _{-0.02}	0.75 ^{0.009} _{-0.009}
A2244	7.10 ^{5.00} _{-2.20}	0.23	0.607 ^{0.016} _{-0.015}	88.7 ^{8.6} _{-8.6}	1773.0 ^{216.0} _{-222.0}	0.82	8.36 ^{5.89} _{-2.60}	2.46 ^{0.38} _{-0.27}	0.47 ^{0.032} _{-0.025}
A2256	6.60 ^{0.40} _{-0.40}	0.05	0.914 ^{0.054} _{-0.047}	413.4 ^{33.1} _{-34.9}	1684.0 ^{189.0} _{-208.0}	0.93	10.51 ^{0.90} _{-0.84}	6.06 ^{0.18} _{-0.17}	0.52 ^{0.007} _{-0.007}
A2255	6.87 ^{0.20} _{-0.20}	0.03	0.797 ^{0.033} _{-0.030}	417.6 ^{30.3} _{-32.6}	1730.0 ^{160.0} _{-174.0}	0.79	9.82 ^{0.50} _{-0.47}	7.02 ^{0.13} _{-0.12}	0.50 ^{0.005} _{-0.005}
A3667	7.00 ^{0.60} _{-0.60}	0.07	0.541 ^{0.008} _{-0.008}	196.5 ^{10.9} _{-13.1}	2589.0 ^{175.0} _{-199.0}	2.36	10.70 ^{0.93} _{-0.93}	2.18 ^{0.06} _{-0.04}	0.44 ^{0.004} _{-0.004}
S1101	3.00 ^{1.20} _{-0.70}	0.55	0.639 ^{0.006} _{-0.007}	39.4 ^{2.2} _{-2.6}	1064.0 ^{70.0} _{-78.0}	0.20	2.23 ^{0.89} _{-0.52}	0.53 ^{0.08} _{-0.04}	0.49 ^{0.019} _{-0.016}
A2589	3.70 ^{2.20} _{-1.10}	0.12	0.596 ^{0.013} _{-0.012}	83.1 ^{6.6} _{-6.8}	1206.0 ^{116.0} _{-121.0}	0.25	2.90 ^{1.73} _{-0.87}	1.15 ^{0.15} _{-0.11}	0.44 ^{0.023} _{-0.019}
A2597	4.40 ^{0.40} _{-0.70}	0.71	0.633 ^{0.008} _{-0.008}	40.8 ^{2.2} _{-2.7}	1296.0 ^{91.0} _{-103.0}	0.35	3.96 ^{0.36} _{-0.63}	0.77 ^{0.07} _{-0.02}	0.49 ^{0.007} _{-0.007}
A2634	3.70 ^{0.28} _{-0.28}	0.02	0.640 ^{0.051} _{-0.043}	256.3 ^{32.8} _{-31.0}	1225.0 ^{208.0} _{-219.0}	0.23	3.05 ^{0.34} _{-0.31}	2.28 ^{0.08} _{-0.06}	0.43 ^{0.007} _{-0.007}
A2657	3.70 ^{0.30} _{-0.30}	0.10	0.556 ^{0.008} _{-0.007}	83.8 ^{5.0} _{-5.9}	1307.0 ^{90.0} _{-105.0}	0.30	2.94 ^{0.24} _{-0.24}	1.16 ^{0.06} _{-0.02}	0.45 ^{0.005} _{-0.004}

Cluster	T [keV]	ρ_0 $\times 10^{-25}$ [g/cm ³]	β	r_c [kpc]	r_{250} [kpc]	M_{b250} $\times 10^{14}$ [M_\odot]	M_{d250} $\times 10^{14}$ [M_\odot]	M_c $\times 10^{15}$ [M_\odot]	λ^{-1} [r_c]
A4038	3.15 ^{0.03} _{-0.03}	0.26	0.541 ^{0.009} _{-0.008}	41.5 ^{3.3} _{-3.7}	1274.0 ^{121.0} _{-134.0}	0.27	2.38 ^{0.05} _{-0.04}	1.01 ^{0.06} _{-0.00}	0.95 ^{0.008} _{-0.010}
A4059	4.40 ^{0.30} _{-0.30}	0.20	0.582 ^{0.010} _{-0.010}	63.4 ^{4.4} _{-5.0}	1324.0 ^{116.0} _{-126.0}	0.33	3.71 ^{0.26} _{-0.26}	1.45 ^{0.06} _{-0.02}	0.51 ^{0.006} _{-0.005}
A2734	3.85 ^{0.62} _{-0.54}	0.06	0.624 ^{0.034} _{-0.029}	149.3 ^{19.4} _{-18.3}	1357.0 ^{226.0} _{-234.0}	0.35	3.53 ^{0.60} _{-0.52}	1.53 ^{0.08} _{-0.05}	0.45 ^{0.009} _{-0.009}
A2877	3.50 ^{2.20} _{-1.10}	0.03	0.566 ^{0.029} _{-0.025}	133.8 ^{14.5} _{-14.1}	943.0 ^{132.0} _{-139.0}	0.11	2.01 ^{1.27} _{-0.64}	1.74 ^{0.25} _{-0.18}	0.40 ^{0.022} _{-0.019}
NGC499	0.72 ^{0.03} _{-0.02}	0.20	0.722 ^{0.034} _{-0.030}	16.9 ^{1.6} _{-1.7}	196.0 ^{27.0} _{-30.0}	0.00	0.11 ^{0.01} _{-0.01}	0.34 ^{0.08} _{-0.01}	0.61 ^{0.009} _{-0.009}
AWM7	3.75 ^{0.09} _{-0.09}	0.09	0.671 ^{0.027} _{-0.025}	121.8 ^{13.7} _{-12.6}	1120.0 ^{157.0} _{-154.0}	0.23	3.06 ^{0.14} _{-0.14}	1.97 ^{0.05} _{-0.02}	0.58 ^{0.007} _{-0.007}
PERSEUS	6.79 ^{0.12} _{-0.12}	0.63	0.540 ^{0.006} _{-0.004}	45.1 ^{2.4} _{-2.9}	2414.0 ^{145.0} _{-189.0}	1.87	9.71 ^{0.20} _{-0.19}	1.86 ^{0.05} _{-0.01}	0.90 ^{0.008} _{-0.010}
S405	4.21 ^{0.67} _{-0.59}	0.02	0.664 ^{0.263} _{-0.133}	323.2 ^{185.0} _{-113.4}	1561.0 ^{1034.0} _{-1165.0}	0.44	4.59 ^{1.96} _{-1.14}	2.64 ^{0.27} _{-0.25}	0.44 ^{0.023} _{-0.021}
3C129	5.60 ^{0.70} _{-0.60}	0.03	0.601 ^{0.260} _{-0.131}	223.9 ^{125.7} _{-76.4}	1567.0 ^{1113.0} _{-1455.0}	0.46	5.67 ^{2.55} _{-1.38}	3.65 ^{0.55} _{-0.29}	0.44 ^{0.029} _{-0.019}
A0539	3.24 ^{0.09} _{-0.09}	0.06	0.561 ^{0.020} _{-0.018}	104.2 ^{10.2} _{-10.3}	1194.0 ^{150.0} _{-158.0}	0.22	2.36 ^{0.11} _{-0.10}	1.35 ^{0.06} _{-0.01}	0.51 ^{0.005} _{-0.005}
S540	2.40 ^{0.38} _{-0.34}	0.08	0.641 ^{0.073} _{-0.051}	91.5 ^{27.0} _{-21.1}	877.0 ^{305.0} _{-305.0}	0.10	1.46 ^{0.29} _{-0.24}	0.90 ^{0.07} _{-0.04}	0.50 ^{0.015} _{-0.013}
A0548w	1.20 ^{0.19} _{-0.17}	0.02	0.666 ^{0.194} _{-0.111}	139.4 ^{63.7} _{-44.4}	593.0 ^{311.0} _{-328.0}	0.03	0.49 ^{0.16} _{-0.11}	0.48 ^{0.09} _{-0.04}	0.43 ^{0.024} _{-0.021}
A0548	3.10 ^{0.10} _{-0.10}	0.05	0.480 ^{0.013} _{-0.013}	83.1 ^{9.2} _{-9.1}	1324.0 ^{177.0} _{-175.0}	0.25	2.15 ^{0.09} _{-0.09}	1.13 ^{0.06} _{-0.01}	0.48 ^{0.005} _{-0.005}
A3395	5.00 ^{0.30} _{-0.30}	0.02	0.981 ^{0.619} _{-0.244}	473.2 ^{270.5} _{-145.4}	1221.0 ^{783.0} _{-977.0}	0.30	5.71 ^{3.65} _{-1.69}	6.12 ^{1.78} _{-0.94}	0.44 ^{0.040} _{-0.029}
UGC03957	2.58 ^{0.41} _{-0.36}	0.09	0.740 ^{0.133} _{-0.086}	100.0 ^{32.0} _{-23.9}	764.0 ^{306.0} _{-339.0}	0.08	1.57 ^{0.38} _{-0.29}	1.33 ^{0.10} _{-0.07}	0.52 ^{0.019} _{-0.016}
PKS0745	7.21 ^{0.11} _{-0.11}	0.97	0.608 ^{0.006} _{-0.006}	50.0 ^{2.5} _{-3.1}	2169.0 ^{137.0} _{-159.0}	1.58	10.43 ^{0.19} _{-0.19}	2.32 ^{0.04} _{-0.01}	1.23 ^{0.009} _{-0.013}
A0644	7.90 ^{0.80} _{-0.80}	0.15	0.700 ^{0.011} _{-0.011}	143.0 ^{7.8} _{-9.4}	1557.0 ^{103.0} _{-119.0}	0.65	9.37 ^{0.96} _{-0.96}	4.23 ^{0.11} _{-0.10}	0.49 ^{0.006} _{-0.006}
S636	1.18 ^{0.19} _{-0.17}	0.01	0.752 ^{0.217} _{-0.123}	242.3 ^{92.1} _{-62.1}	742.0 ^{323.0} _{-336.0}	0.04	0.65 ^{0.22} _{-0.15}	0.64 ^{0.11} _{-0.07}	0.42 ^{0.023} _{-0.020}
A1413	7.32 ^{0.26} _{-0.24}	0.19	0.660 ^{0.017} _{-0.015}	126.1 ^{10.0} _{-10.5}	1794.0 ^{179.0} _{-194.0}	0.94	9.46 ^{0.42} _{-0.38}	3.71 ^{0.04} _{-0.04}	0.62 ^{0.007} _{-0.007}
M49	0.95 ^{0.02} _{-0.01}	0.26	0.592 ^{0.007} _{-0.007}	7.7 ^{0.8} _{-0.8}	177.0 ^{19.0} _{-20.0}	0.00	0.11 ^{0.00} _{-0.00}	0.74 ^{0.07} _{-0.01}	1.04 ^{0.012} _{-0.014}
A3528n	3.40 ^{1.66} _{-0.64}	0.07	0.621 ^{0.034} _{-0.030}	125.4 ^{13.1} _{-13.3}	1181.0 ^{179.0} _{-193.0}	0.25	2.71 ^{1.33} _{-0.53}	1.16 ^{0.15} _{-0.10}	0.44 ^{0.021} _{-0.017}
A3528s	3.15 ^{0.89} _{-0.59}	0.09	0.463 ^{0.013} _{-0.012}	71.1 ^{7.0} _{-6.9}	1872.0 ^{244.0} _{-250.0}	0.72	2.99 ^{0.85} _{-0.57}	0.61 ^{0.07} _{-0.02}	0.41 ^{0.009} _{-0.009}
A3530	3.89 ^{0.27} _{-0.25}	0.03	0.773 ^{0.114} _{-0.085}	296.5 ^{54.3} _{-46.1}	1150.0 ^{282.0} _{-308.0}	0.28	3.56 ^{0.58} _{-0.46}	2.50 ^{0.14} _{-0.11}	0.46 ^{0.011} _{-0.010}
A3532	4.58 ^{0.19} _{-0.17}	0.05	0.653 ^{0.034} _{-0.029}	198.6 ^{20.8} _{-20.3}	1372.0 ^{188.0} _{-199.0}	0.42	4.41 ^{0.29} _{-0.26}	2.42 ^{0.05} _{-0.05}	0.50 ^{0.006} _{-0.006}
A1689	9.23 ^{0.28} _{-0.28}	0.33	0.690 ^{0.011} _{-0.011}	114.8 ^{6.9} _{-7.7}	1898.0 ^{143.0} _{-154.0}	1.21	13.21 ^{0.45} _{-0.45}	4.87 ^{0.05} _{-0.05}	0.69 ^{0.007} _{-0.007}
A3560	3.16 ^{0.51} _{-0.44}	0.03	0.566 ^{0.033} _{-0.029}	180.3 ^{22.5} _{-21.6}	1402.0 ^{230.0} _{-240.0}	0.32	2.71 ^{0.46} _{-0.40}	1.16 ^{0.07} _{-0.04}	0.42 ^{0.008} _{-0.008}
A1775	3.69 ^{0.20} _{-0.11}	0.06	0.673 ^{0.026} _{-0.023}	183.1 ^{15.5} _{-16.3}	1391.0 ^{153.0} _{-167.0}	0.41	3.73 ^{0.25} _{-0.17}	1.66 ^{0.06} _{-0.03}	0.52 ^{0.006} _{-0.005}
A1800	4.02 ^{0.64} _{-0.56}	0.04	0.766 ^{0.308} _{-0.139}	276.1 ^{157.5} _{-94.2}	1284.0 ^{825.0} _{-949.0}	0.38	4.15 ^{1.80} _{-0.97}	2.30 ^{0.32} _{-0.22}	0.48 ^{0.032} _{-0.024}
A1914	10.53 ^{0.51} _{-0.50}	0.22	0.751 ^{0.018} _{-0.017}	162.7 ^{10.4} _{-11.6}	1768.0 ^{148.0} _{-162.0}	1.09	15.21 ^{0.82} _{-0.80}	7.28 ^{0.10} _{-0.10}	0.60 ^{0.006} _{-0.006}
NGC5813	0.52 ^{0.08} _{-0.07}	0.18	0.766 ^{0.179} _{-0.103}	17.6 ^{6.4} _{-4.3}	166.0 ^{79.0} _{-97.0}	0.00	0.07 ^{0.02} _{-0.01}	0.19 ^{0.08} _{-0.01}	0.54 ^{0.025} _{-0.022}

Cluster	T [keV]	ρ_0 $\times 10^{-25}$ [g/cm ³]	β	r_c [kpc]	r_{250} [kpc]	M_{b250} $\times 10^{14}$ [M_\odot]	M_{d250} $\times 10^{14}$ [M_\odot]	M_c $\times 10^{15}$ [M_\odot]	λ^{-1} [r_c]
NGC5846	0.82 ^{0.01} _{-0.01}	0.47	0.599 ^{0.016} _{-0.015}	4.9 ^{0.7} _{-0.8}	152.0 ^{26.0} _{-27.0}	0.00	0.08 ^{0.00} _{-0.00}	0.60 ^{0.07} _{-0.01}	1.35 ^{0.018} _{-0.022}
A2151w	2.40 ^{0.06} _{-0.06}	0.16	0.564 ^{0.014} _{-0.013}	47.9 ^{4.1} _{-4.4}	957.0 ^{105.0} _{-114.0}	0.12	1.42 ^{0.05} _{-0.05}	0.75 ^{0.07} _{-0.01}	0.61 ^{0.007} _{-0.006}
A3627	6.02 ^{0.08} _{-0.08}	0.04	0.555 ^{0.056} _{-0.044}	210.6 ^{40.4} _{-36.5}	1830.0 ^{474.0} _{-515.0}	0.84	6.62 ^{0.67} _{-0.53}	3.01 ^{0.08} _{-0.07}	0.47 ^{0.009} _{-0.008}
TRIANGUL	9.60 ^{0.60} _{-0.60}	0.10	0.610 ^{0.010} _{-0.010}	196.5 ^{11.4} _{-13.1}	2385.0 ^{169.0} _{-187.0}	2.04	15.22 ^{0.98} _{-0.98}	4.56 ^{0.07} _{-0.06}	0.49 ^{0.005} _{-0.004}
OPHIUCHU	10.26 ^{0.32} _{-0.32}	0.13	0.747 ^{0.035} _{-0.032}	196.5 ^{18.2} _{-19.0}	1701.0 ^{224.0} _{-240.0}	0.93	14.12 ^{0.80} _{-0.75}	9.17 ^{0.15} _{-0.14}	0.59 ^{0.007} _{-0.006}
ZwC174	5.23 ^{0.84} _{-0.73}	0.10	0.717 ^{0.073} _{-0.053}	163.4 ^{33.1} _{-28.3}	1354.0 ^{349.0} _{-378.0}	0.44	5.49 ^{1.04} _{-0.87}	2.67 ^{0.14} _{-0.12}	0.51 ^{0.014} _{-0.013}
A2319	8.80 ^{0.50} _{-0.50}	0.10	0.591 ^{0.013} _{-0.012}	200.7 ^{13.5} _{-15.0}	2657.0 ^{228.0} _{-250.0}	2.70	15.08 ^{0.92} _{-0.91}	3.54 ^{0.05} _{-0.05}	0.50 ^{0.005} _{-0.005}
A3695	5.29 ^{0.85} _{-0.74}	0.04	0.642 ^{0.259} _{-0.117}	281.0 ^{179.3} _{-106.1}	1887.0 ^{1379.0} _{-1652.0}	0.96	6.88 ^{2.99} _{-1.59}	2.50 ^{0.27} _{-0.21}	0.47 ^{0.029} _{-0.022}
IIZw108	3.44 ^{0.55} _{-0.48}	0.03	0.662 ^{0.167} _{-0.097}	257.0 ^{112.5} _{-75.3}	1327.0 ^{670.0} _{-695.0}	0.36	3.20 ^{0.96} _{-0.65}	1.53 ^{0.13} _{-0.10}	0.45 ^{0.019} _{-0.017}
A3822	4.90 ^{0.78} _{-0.69}	0.04	0.639 ^{0.150} _{-0.093}	247.2 ^{113.2} _{-79.4}	1675.0 ^{904.0} _{-942.0}	0.67	5.63 ^{1.60} _{-1.15}	2.45 ^{0.19} _{-0.15}	0.47 ^{0.021} _{-0.019}
A3827	7.08 ^{1.13} _{-0.99}	0.05	0.989 ^{0.410} _{-0.192}	417.6 ^{175.5} _{-106.5}	1515.0 ^{762.0} _{-977.0}	0.72	10.82 ^{4.82} _{-2.67}	7.99 ^{2.08} _{-0.86}	0.51 ^{0.045} _{-0.024}
A3888	8.84 ^{1.41} _{-1.24}	0.10	0.928 ^{0.084} _{-0.066}	282.4 ^{34.5} _{-32.4}	1455.0 ^{252.0} _{-281.0}	0.70	12.62 ^{2.32} _{-1.99}	9.10 ^{0.61} _{-0.47}	0.53 ^{0.015} _{-0.012}
A3921	5.73 ^{0.24} _{-0.23}	0.07	0.762 ^{0.036} _{-0.030}	231.0 ^{20.7} _{-20.8}	1435.0 ^{167.0} _{-182.0}	0.54	6.70 ^{0.42} _{-0.38}	3.97 ^{0.08} _{-0.07}	0.54 ^{0.007} _{-0.006}
HCG94	3.45 ^{0.30} _{-0.30}	0.11	0.514 ^{0.007} _{-0.006}	60.6 ^{3.8} _{-4.4}	1237.0 ^{89.0} _{-104.0}	0.25	2.40 ^{0.21} _{-0.21}	1.01 ^{0.06} _{-0.02}	0.44 ^{0.005} _{-0.004}
RXJ2344	4.73 ^{0.76} _{-0.66}	0.07	0.807 ^{0.033} _{-0.030}	212.0 ^{16.7} _{-17.4}	1222.0 ^{127.0} _{-135.0}	0.33	4.97 ^{0.82} _{-0.72}	2.85 ^{0.14} _{-0.12}	0.48 ^{0.010} _{-0.009}

Table 1. The table presents various cluster properties, including cluster temperature (T), central density (ρ_0), β parameter, and core radius (r_c). These data points have been sourced from [25]. Additionally, the table includes the cluster’s outer radius (r_{out}), defined as the radius where the surface intensity reaches 250 times the ambient intensity. It also lists the total baryonic mass within the cluster (M_b) and the cluster’s dynamical mass (M_d) as calculated using Newtonian dynamics. The upper and lower standard deviations have been computed based on the standard deviations of T , β , and r_c . Furthermore, the table includes values for M_c and λ^{-1} derived from an MCMC analysis. Notably, λ^{-1} is expressed relative to r_c , with the observation that λ^{-1} tends to be approximately half the size of r_c .

Cluster	ρ_0	r_c [kpc]	r_{2500} [kpc]	M_{b2500} $\times 10^{13}$ [M_\odot]	M_{d2500} $\times 10^{14}$ [M_\odot]	α	Q	λ^{-1} [kpc]
2A0335	$31.0^{2.6}_{-2.1}$	$204.0^{28.0}_{-22.0}$	517.8	$1.59^{0.02}_{-0.02}$	1.24 ± 0.05	0.06 ± 0.01	10.51 ± 0.21	4.53 ± 1.79
3C295	$50.9^{9.9}_{-6.7}$	$236.0^{96.0}_{-64.0}$	875.0	$4.85^{0.47}_{-0.45}$	3.30 ± 0.40	0.17 ± 0.03	6.96 ± 0.56	11.97 ± 5.03
3C388	$23.7^{2.5}_{-1.5}$	$127.0^{38.0}_{-27.0}$	757.2	$1.73^{0.13}_{-0.13}$	1.20 ± 0.17	0.41 ± 0.04	7.55 ± 0.66	19.04 ± 3.50
3C401	$30.3^{13.0}_{-5.8}$	$210.0^{180.0}_{-82.0}$	816.2	$2.17^{0.32}_{-0.27}$	2.00 ± 0.46	0.32 ± 0.08	9.62 ± 1.54	19.84 ± 11.7
A85	$51.1^{5.0}_{-4.0}$	$381.0^{66.0}_{-53.0}$	640.4	$3.76^{0.05}_{-0.05}$	2.50 ± 0.09	0.18 ± 0.01	7.79 ± 0.13	7.65 ± 1.69
A133	$36.4^{6.9}_{-3.6}$	$314.0^{130.0}_{-75.0}$	654.1	$2.06^{0.06}_{-0.06}$	1.80 ± 0.12	0.24 ± 0.02	9.48 ± 0.36	24.04 ± 3.14
A1795	$55.0^{1.6}_{-1.6}$	$373.0^{21.0}_{-21.0}$	892.2	$5.75^{0.17}_{-0.15}$	3.81 ± 0.05	0.14 ± 0.00	7.23 ± 0.11	14.72 ± 0.73
A1835	$95.7^{3.4}_{-3.7}$	$439.0^{29.0}_{-31.0}$	1550.8	$19.00^{0.32}_{-0.32}$	11.00 ± 0.49	0.08 ± 0.01	6.65 ± 0.14	11.78 ± 0.95
A2029	$68.8^{3.9}_{-3.4}$	$304.0^{30.0}_{-26.0}$	969.7	$8.95^{0.11}_{-0.11}$	5.04 ± 0.11	0.19 ± 0.00	6.81 ± 0.18	2.58 ± 0.87
A2052	$27.3^{0.48}_{-0.46}$	$198.0^{9.7}_{-9.6}$	533.0	$1.39^{0.08}_{-0.08}$	1.12 ± 0.01	0.30 ± 0.01	8.45 ± 0.22	22.66 ± 0.77
A2199	$45.6^{2.8}_{-2.1}$	$363.0^{36.0}_{-26.0}$	444.2	$1.34^{0.01}_{-0.01}$	1.48 ± 0.02	0.17 ± 0.01	10.47 ± 0.32	1.90 ± 0.53
A2204	$97.9^{3.6}_{-2.7}$	$305.0^{54.0}_{-45.0}$	1581.2	$17.40^{0.56}_{-0.56}$	10.50 ± 0.12	0.27 ± 0.01	6.30 ± 0.17	61.24 ± 3.00
A2597	$39.1^{1.3}_{-1.5}$	$234.0^{20.0}_{-25.0}$	965.5	$3.95^{0.15}_{-0.15}$	2.73 ± 0.05	0.16 ± 0.01	7.65 ± 0.17	24.91 ± 1.21
A262	$14.0^{0.52}_{-0.45}$	$134.0^{11.0}_{-9.7}$	357.2	$0.50^{0.01}_{-0.01}$	0.39 ± 0.01	0.37 ± 0.01	8.82 ± 0.24	11.35 ± 0.76
A4059	$40.2^{1.7}_{-1.5}$	$237.0^{29.0}_{-25.0}$	825.9	$2.46^{0.07}_{-0.07}$	2.50 ± 0.09	0.23 ± 0.01	10.75 ± 0.22	6.30 ± 3.04
A478	$86.7^{6.6}_{-5.5}$	$553.0^{68.0}_{-56.0}$	1228.5	$11.80^{0.28}_{-0.28}$	8.30 ± 0.26	0.11 ± 0.00	6.54 ± 0.15	3.07 ± 1.17
A496	$37.9^{0.66}_{-0.62}$	$131.0^{26.0}_{-21.0}$	714.4	$2.65^{0.08}_{-0.09}$	1.80 ± 0.07	0.46 ± 0.02	7.20 ± 0.22	39.45 ± 3.62
Centaurus	$35.1^{0.27}_{-0.38}$	276	249.0	$0.32^{0.00}_{-0.00}$	0.62 ± 0.01	0.25 ± 0.01	20.32 ± 0.51	17.75 ± 0.89
Cygnus A	$45.2^{4.5}_{-2.1}$	$145.0^{70.0}_{-43.0}$	814.7	$5.90^{0.07}_{-0.06}$	2.50 ± 0.12	0.48 ± 0.02	4.91 ± 0.19	49.07 ± 3.73
HCG62	$7.02^{1.9}_{-0.8}$	$48.6^{37.0}_{-19.0}$	192.9	$0.05^{0.00}_{-0.00}$	0.10 ± 0.00	0.79 ± 0.05	17.67 ± 0.70	28.95 ± 2.47
Hercules A	$53.7^{14.0}_{-3.4}$	$135.0^{190.0}_{-85.0}$	1114.7	$5.62^{0.69}_{-0.70}$	3.50 ± 0.23	0.50 ± 0.06	6.52 ± 0.39	75.12 ± 15.3
Hydra A	$35.3^{1.2}_{-0.65}$	$341.0^{25.0}_{-24.0}$	789.7	$3.16^{0.05}_{-0.05}$	2.16 ± 0.05	0.18 ± 0.01	6.40 ± 0.15	25.67 ± 0.88
MACSJ0159	$125.0^{100.0}_{-39.0}$	$700.0^{730.0}_{-270.0}$	1311.7	$15.80^{0.27}_{-0.27}$	13.00 ± 0.80	0.07 ± 0.02	8.10 ± 0.38	12.16 ± 3.10
MACSJ0242	$57.9^{63.0}_{-12.0}$	$258.0^{230.0}_{-81.0}$	679.0	$4.97^{0.11}_{-0.26}$	3.00 ± 0.57	0.20 ± 0.18	6.04 ± 1.18	25.15 ± 21.4
MACSJ0429	$54.5^{14.0}_{-6.8}$	$202.0^{100.0}_{-51.0}$	791.1	$5.72^{0.34}_{-0.34}$	3.10 ± 0.45	0.21 ± 0.04	6.15 ± 0.55	12.55 ± 6.34
MACSJ0913	$71.7^{18.0}_{-8.6}$	$305.0^{120.0}_{-57.0}$	827.3	$5.51^{0.27}_{-0.26}$	4.60 ± 0.50	0.03 ± 0.01	9.04 ± 0.41	5.59 ± 2.71
MACSJ1423	$70.6^{8.1}_{-6.0}$	$211.0^{59.0}_{-46.0}$	1263.4	$10.70^{0.87}_{-0.84}$	5.80 ± 0.58	0.24 ± 0.03	6.12 ± 0.41	23.50 ± 3.97
MACSJ1720	$67.8^{18.0}_{-16.0}$	$405.0^{170.0}_{-150.0}$	796.6	$6.48^{0.24}_{-0.24}$	4.20 ± 0.52	0.15 ± 0.04	6.52 ± 0.51	15.82 ± 8.62
MACSJ1931	$126.0^{43.0}_{-22.0}$	$851.0^{390.0}_{-200.0}$	1721.4	$19.90^{1.90}_{-1.40}$	17.00 ± 1.40	0.01 ± 0.00	7.02 ± 0.17	13.59 ± 1.00

Cluster	ρ_0	r_c [kpc]	r_{2500} [kpc]	M_{b2500} $\times 10^{13}$ [M_\odot]	M_{d2500} $\times 10^{14}$ [M_\odot]	α	Q	λ^{-1} [kpc]
MACSJ2046	$52.9^{16.0}_{-5.3}$	$210.0^{130.0}_{-45.0}$	957.4	$7.82^{1.10}_{-1.20}$	3.60 ± 0.76	0.35 ± 0.13	4.93 ± 0.81	49.03 ± 29.0
MACSJ2140	$51.1^{5.2}_{-2.7}$	$176.0^{36.0}_{-30.0}$	920.7	$5.73^{0.34}_{-0.39}$	3.20 ± 0.34	0.14 ± 0.02	6.90 ± 0.35	6.24 ± 2.68
MKW3S	$34.9^{12.0}_{-4.3}$	$214.0^{210.0}_{-90.0}$	567.3	$1.41^{0.02}_{-0.02}$	1.50 ± 0.15	0.22 ± 0.04	11.01 ± 0.56	18.07 ± 9.30
MS0735	$66.2^{13.0}_{-3.0}$	$368.0^{27.0}_{-140.0}$	1549.8	$11.10^{0.35}_{-0.39}$	7.40 ± 0.36	0.20 ± 0.03	7.02 ± 0.28	61.25 ± 23.2
NGC1550	$9.62^{0.25}_{-0.16}$	$58.7^{5.3}_{-3.7}$	241.6	$0.13^{0.01}_{-0.01}$	0.17 ± 0.01	0.40 ± 0.01	13.88 ± 0.31	8.71 ± 0.46
NGC5044	$6.97^{0.2}_{-0.16}$	$45.1^{5.4}_{-4.7}$	217.7	$0.09^{0.00}_{-0.00}$	0.11 ± 0.00	0.44 ± 0.01	12.99 ± 0.36	11.99 ± 0.63
NGC507	$10.4^{2.4}_{-1.5}$	$115.0^{77.0}_{-34.0}$	167.0	$0.07^{0.00}_{-0.00}$	0.13 ± 0.01	0.26 ± 0.01	23.79 ± 0.70	3.12 ± 1.43
Perseus	$39.3^{0.5}_{-0.46}$	$205.0^{4.9}_{-4.6}$	329.9	$1.44^{0.00}_{-0.00}$	0.99 ± 0.01	0.14 ± 0.00	7.91 ± 0.33	2.66 ± 0.98
PKS0745	$68.9^{5.3}_{-4.5}$	$351.0^{50.0}_{-42.0}$	1115.8	$10.10^{0.15}_{-0.15}$	5.80 ± 0.30	0.08 ± 0.01	6.63 ± 0.14	5.60 ± 2.58
PKS1404	$14.4^{0.41}_{-0.37}$	$98.2^{6.0}_{-5.4}$	260.3	$0.24^{0.00}_{-0.00}$	0.29 ± 0.01	0.25 ± 0.04	15.35 ± 1.35	3.33 ± 2.08
RBS797	$102.0^{29.0}_{-15.0}$	$421.0^{230.0}_{-110.0}$	1715.1	$16.50^{1.90}_{-2.00}$	13.00 ± 1.20	0.02 ± 0.01	8.41 ± 0.29	14.22 ± 4.76
RXJ1532	$93.5^{44.0}_{-17.0}$	$502.0^{380.0}_{-150.0}$	969.2	$8.17^{0.24}_{-0.23}$	7.00 ± 0.89	0.02 ± 0.01	7.52 ± 0.19	18.45 ± 3.07
Sersic159	$29.6^{2.1}_{-1.8}$	$233.0^{29.0}_{-26.0}$	552.9	$1.51^{0.03}_{-0.03}$	1.30 ± 0.05	0.10 ± 0.00	9.46 ± 0.20	3.53 ± 1.45
Zw2701	$48.8^{6.1}_{-3.5}$	$248.0^{79.0}_{-49.0}$	1098.2	$5.51^{0.18}_{-0.18}$	3.80 ± 0.31	0.19 ± 0.02	7.83 ± 0.40	14.67 ± 4.93
Zw3146	$106.0^{33.0}_{-21.0}$	$738.0^{310.0}_{-190.0}$	2578.5	$28.50^{0.94}_{-1.20}$	21.00 ± 1.90	0.03 ± 0.01	6.07 ± 0.19	2.85 ± 1.06

Table 2. The provided table presents various cluster properties, including cluster central density (ρ_0), core radius (r_c), r_{2500} ; the calculated quantities M_{b2500} , M_{d2500} , and the fitted quantities α , Q , λ^{-1} . These data points have been sourced from [32]. The unit of ρ_0 is so chosen that $A = 4\pi G \rho_0 r_c^2 \mu m_H$ is in keV unit.